Performance Analysis of P2MP Hybrid FSO/RF Network

by

Yaseen Akbar Ansari
B.Sc., Sir Syed University Karachi, 2010

A thesis submitted in partial fulfilment of the
requirements for the Degree of

MASTER OF APPLIED SCIENCE

in the Department of Electrical and Computer Engineering

Performance Analysis of P2MP Hybrid FSO/RF Network

by

Yaseen Akbar Ansari
B.Sc., Sir Syed University Karachi, 2010

Supervisory Committee

---

Dr. Fayez Gebali, Supervisor
(Department of Electrical and Computer Engineering)

---

Dr. M. Watheq El-Kharashi, Member
(Department of Electrical and Computer Engineering)

## ABSTRACT

Free space optics (FSO) technology is proving to be an exceptionally beneficial supplement to conventional Fiber Optics and radio frequency (RF) links. FSO and RF links are greatly affected by atmospheric conditions. Hybrid FSO/RF systems have emerged as a promising solution for high data rate wireless communication. FSO technology can be used effectively in multi-user scenarios to support Point-to-Multi-Point (P2MP) networks. In this work we present and analyse a P2MP Hybrid FSO/RF network that uses a number of FSO links for data transmission from the central node to different remote nodes of the network. A common backup RF link is used by the central node to transmit data to any of the remote nodes in case of failure of any FSO links. Each remote node is assigned a transmit buffer at the central node for the downlink transmission. We deploy a non-equal priority protocol and $p$-persistent strategy for nodes accessing the RF link and consider the back up RF transmission link with lower frame transmission rates as compared to the FSO link. Under different atmospheric conditions, we also study various performance metrics of the network. We study the throughput from the central node to the remote nodes individually as well as the following: the average transmit buffer size, the frame queuing delay in the transmit buffers, the efficiency of the queuing systems and the frame loss probability.

# Contents

# List of Tables

# List of Figures

# List of Acronyms

| | |
|---|---|
| 5G | Fifth Generation |
| FSO | Free Space Optical |
| IR | Infra Red |
| LADEE | Lunar Atmosphere and Dust Environment Explorer |
| LAN | Local Area Network |
| LED | Light Emitting Diode |
| Li-Fi | Light-Fidelity |
| LLCD | Lunar Laser Communication Demonstration |
| LTE | Long Term Evolution |
| NASA | National Aeronautics and Space Administration |
| MMW | Millimeter Wavelength |
| OWC | Optical Wireless Communication |
| P2MP | Point-to-Multi-Point |
| P2P | Point-to-Point |
| RF | Radio Frequency |
| SNR | Signal to Noise Ratio |
| UV | Ultra Violet |
| VLC | Visible Light Communications |
| Wi-Fi | Wireless Fidelity |
| WISP | Wireless Internet Service Provider |

# ACKNOWLEDGEMENT

I would like to thank:

**My Parents** for their continuous prayers, love, patience, support, motivation and assurance during difficult and frustrating times.

**My supervisor Dr. Fayez Gebali** for his advice and support during my work under his supervision. It would not have been possible to complete my thesis without his invaluable knowledge, guidance, constructive comments and suggestions during all stages of my study.

# DEDICATION

*To my parents, my father Mr. Mohammad Akbar and mother, Reshma Nasreen for always allowing me to achieve what I desire and for always being there, with their never ending support, love and prayers.*

*To my supervisor, Dr. Fayez Gebali for his constant guidance and support, he is one of the most learned, kindest and helpful person I have known, I wish him good health, joy and prosperity.*

*To my fiancée, for her encouragement and motivation.*

# Chapter 1

# Introduction

## 1.1 Overview

The constant need for higher data rates in support of the demanding wireless communication applications has fostered the drive of developing new technologies in the field of Optical Wireless Communication (OWC) and Millimetre Wavelength (MMW) radio frequency (RF). OWC refers to data transmission in unguided propagation media through the use of an optical carrier, and is further categorized into three main types, which are Free-Space Optical (FSO) communications, Visible Light Communications (VLC), and Ultra-Violet (UV) Communications. This work is on a hybrid system using Free Space Optical (FSO) and millimeter wavelength (MMW) radio frequency (RF) communication technologies. Operating at the unlicensed optical and 60 GHz frequencies, FSO and MMW RF systems offer the potential of broadband capacity (up to a few Gbps) at a low cost and over distances of up to a few kilometers [6], [7]. Despite their common features, FSO and MMW RF systems are not affected in the same way by atmospheric and weather effects. Several studies have shown that fog is the main attenuation factor in FSO links [8], [9], while rain does not cause significant effects. On the contrary, 60 GHz RF links are susceptible to heavy rain conditions and oxygen absorption [7]-[9], while fog has no particular effect.

The complementary nature of FSO and MMW RF links led to various approaches in hybrid FSO/RF data transmission systems. Hybrid FSO/RF data transmission systems showed great outage performance and high data link reliability in all weather conditions, while maintaining the high data rate transmissions. Some previously introduced Hybrid FSO/RF approaches include diversity combining hybrid FSO/RF

systems [10], switch-over hybrid FSO/RF systems [11] and hybrid FSO/RF systems with adaptive combining [12] and cross layer analysis of P2MP Hybrid FSO/RF network [13]. In this work a novel architecture of P2MP hybrid Free Space Optic(FSO)/Radio Frequency(RF) wireless systems is presented with a realistic approach of back up RF link having a lower data rate and using $p$-persistent strategy. We presented an analytical model with a detailed study of various performance matrices of the proposed P2MP Hybrid system. In the next section, we present the challenges associated with using this technology, as well as our proposed solutions to these challenges.

## 1.2 Motivation for this Thesis

Due to the considerable demand for wireless bandwidth, radio frequency resources have become cluttered and expensive. Communicating over the optical domain, with its nearly boundless bandwidth has proven to be a viable alternative for high-speed wireless connectivity. As a result, Free-Space Optical (FSO) technology has gained an increasing interest in data transmission [6] [7], owing its unique features including: 1) higher data rate, compared to radio frequency (RF) technology, 2) high transmission security, 3) large unregulated spectrum, and 4) faster and cheaper deployments, compared to fiber optics [13].

However, FSO technology cannot replace current RF communication systems. The requirement of line-of-sight limits the implementation of FSO links. Moreover, channel impairments such as visibility, atmospheric scintillation, background light interference and pointing issues can seriously affect the communication quality. An attractive solution is to build a wireless system including both FSO and reliable lower-rate RF links, forming so-called hybrid FSO/RF communication systems.

Most of the current literature on FSO systems are mainly limited to point-to-point data transmissions. However, FSO technology can also be used effectively in multiuser scenarios [5], [14] to support Point-to-Multipoint (P2MP) topologies. P2MP topology is a common network architecture for outdoor wireless networks to connect multiple locations to one single central location or node.

In this thesis, we present an in-depth analyses on hybrid P2MP FSO/RF wireless systems, in which the FSO channel acts as the main link between a central and remote nodes for data transmission and RF as a back up link with lower data rate. We hope

to provide researchers a useful tool, which can be utilized for performance calculations and implementation of hybrid FSO/RF systems for real-world application.

## 1.3 Contributions

Hybrid P2MP FSO/RF network performance can be evaluated with two general approaches. One approach is to conduct experiments, which are typically costly and time consuming. On the other hand, analytical system performance evaluation can be a good alternative to experiments, and the obtained numerical results can be used efficiently at the initial stages of system design. In this thesis, we will focus on efficient analytical performance evaluation of the proposed hybrid P2MP FSO/RF systems, which will provide important engineering insights into hybrid FSO/RF systems design and later prove our model with the Monte Carlo numeric simulation.

The major contributions of this thesis are as following:

- A Markov chain model of the proposed network is developed.
- Non-equal priority protocol when transmitting to a remote node using RF link is introduced.
- The proposed model using the Monte Carlo method is Verified.

## 1.4 Thesis Organization

Chapter 1 introduces the reader to the subject and scope of the research. The motivation, objective and the contributions of the research are discussed.

Chapter 2 describes the background and fundamentals of FSO and RF systems. Real world examples and different types of FSO systems are discussed to further develop the readers interest. Further, chapter 2 will discuss shortcomings of conventional FSO systems and presents Hybrid FSO/RF as an attractive alternative solution. Lastly, we present our thesis work, Hybrid P2MP FSO/RF systems.

Chapter 3 describes the P2MP hybrid FSO/RF transmission system in detail. The Markovian chain model for the network is presented with different data rates of FSO and RF links. Different performance metric calculations such as throughput, average transmit buffer size, queuing delay, efficiency of the queuing system and loss probability of frame are defined.

Chapter 4 describes parameters used to evaluate the performance of P2MP hybrid FSO/RF transmission system in analytical simulation. Chapter 4 also explains the Monte Carlo method and the algorithm used for numeric simulation. Simulation results are in detail discussed.

Chapter 5 has the concluding statements and a short description of the work and what was achieved through the course of this work.

# Chapter 2

# Literature Review and FSO/RF Background

## 2.1 Free Space Optic Communication

Free Space Optic (FSO) communication is an old communication technology that has existed for thousands of years. In ancient times, soldiers used polished shields and smoke to send signals to remote locations. For many centuries ships have been using blinking lights to communicate with other ships. These are all forms of optical communication.

At present, FSO technology is gaining in interest for point-to-point data transmission links, owing to its high data rate, high transmission security, large unregulated spectrum compared to Radio Frequency (RF) technology, and fast and cheap installation, compared to fiber optics [15].

An example can be taken from the real world incident, when the World Trade Center towers collapsed on September $ll^{th}$, 2001, and all the communication networks for corporations located within the buildings were also destroyed. Hundreds of thousands of dollars were lost due to the down-time. Wireless broadband providers who were using FSO technology were able to get their data networks up and running in a fraction of time [15].

We can divide FSO communication technologies into three categories: outer space, indoor and terrestrial applications.

Outer space optical communications field uses laser communication between satellites or spacecraft. The communication range is on the order of thousands of kilo-

metres. NASA recently launched the Lunar Laser Communication Demonstration (LLCD) project [16], which is the longest-range and fastest laser communication link ever built with a proposed data rate of 622Mbps. The objective is to establish a two-way communication link using lasers between an earth ground station and the Lunar Atmosphere and Dust Environment Explorer (LADEE) spacecraft in Lunar orbit [16].

Another emerging area of FSO research is indoor local area network (LAN) communications, called Li-Fi or Visible Light Communications (VLC). This technology uses visible light emitted from LEDs for communication. The interference between two Li-Fi systems is quite small, in contrast with conventional RF based indoor wireless system, and the cost and size of transceivers are also much lower compared with those of the RF counterpart (Wi-Fi) [17]. Based on the latest research, a data rate over 25 Gbps for stationary users and 22.2 Gbps for a mobile user has been achieved; these are reported highest data rates achieved using VLC technology [18].

Our thesis work is based on terrestrial FSO applications. Point-to-point FSO links are famous for terrestrial applications. FSO links can be used to connect one Local Area Network (LAN) to another LAN and subsequently connect a physical to Backbone networks with optical fibers as shown in Fig. 2.1. In Fig. 2.1 the black arrows are FSO links, and can also be used to different locations within one local area network using mesh architecture [19].

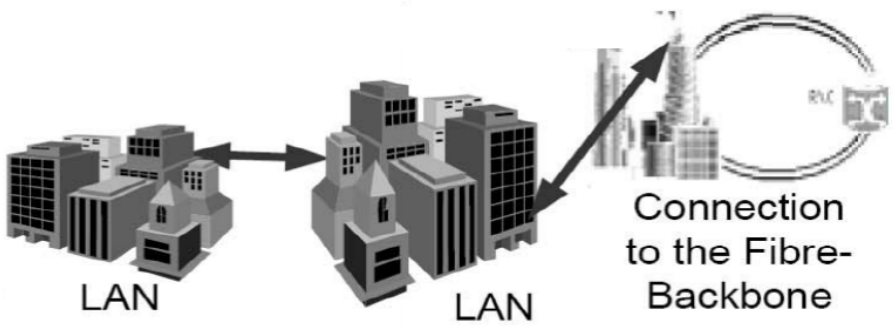


Figure 2.1: LAN-to-LAN FSO connectivity with fiber optic cable [1]

.

FSO can also be used as last-mile applications to connect end users to a broadband network backbone [20]. FSO links can also be used as a robust outdoor back haul solution for small radio cells, such as WiFi, LTE and 5G as shown in Fig. 2.2, where the red arrows are FSO links.

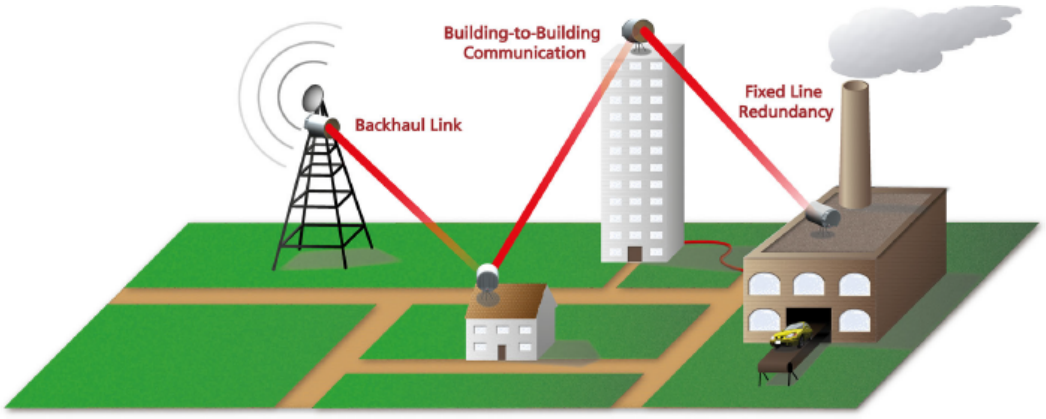


Figure 2.2: Point-to-point backhaul FSO link [2]

.

An FSO transmission system consists of an optical transmitter and an optical receiver which uses the atmosphere as the transmission medium for the optical signal (normally, a laser beam) as shown in Fig 2.3.

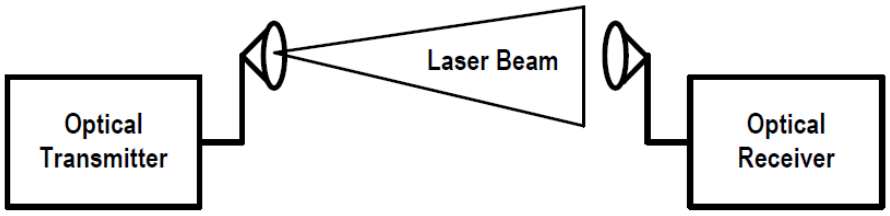


Figure 2.3: FSO system block diagram [3]

.

The optical signal transmitting through the atmosphere is greatly affected by fading due to atmospheric turbulences and pointing errors [4], as shown in Fig. 2.4. Turbulence-induced fading, known as scintillation, causes irradiance fluctuations in the received optical signal as a result of variations in the atmospheric refractive index. Dynamic wind loads and weak earthquakes can cause vibrations of the transmitted optical beam, which also causes random irradiance fluctuations in the received optical signal. Moreover, the optical power is attenuated as the distance between the transmitter and the receiver increases due to a constant loss related to the weather condition [13].

## 2.2 Hybrid FSO/RF Communication System

An attractive solution to the shortcomings of FSO link, as mentioned in the last section, is to build a wireless system including both FSO and Milli-Meter Wavelength (MMW) RF links, forming so-called hybrid FSO/RF communication systems. This hybrid system significantly improves the performance of FSO links.

This is due to the fact that FSO and RF links are affected quite differently by atmospheric and weather effects. FSO links suffer from extremely high attenuation in the presence of fog but are less affected by rain. In contrast, fog has practically no effect on MMW RF links but rain substantially increases link attenuation. Similarly, while atmospheric turbulence is the main cause of small-scale fading in FSO links [13], RF links are impaired by fading due to multipath propagation [21]. Besides the high data rates comparable to FSO links, MMW RF links offer other similar advantages

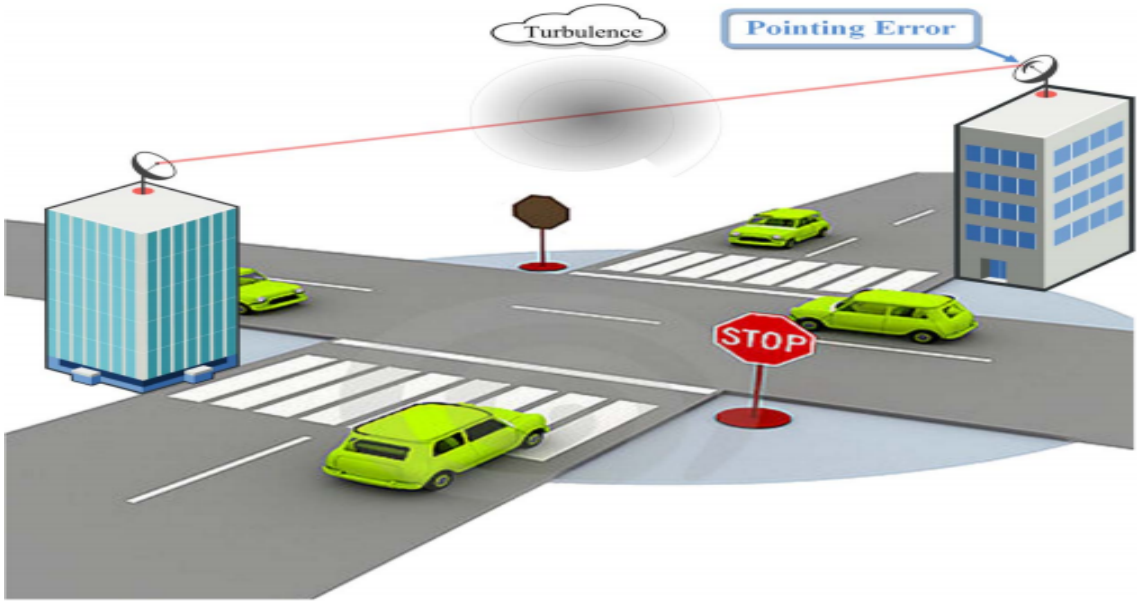


Figure 2.4: Atmospheric turbulence and pointing error in FSO system[4]

.

to FSO links of deployment flexibility, license free operation, and inherent security due to high link attenuation [3].

Previously, two main approaches were presented in implementing hybrid FSO/RF systems. One approach is the switch-over hybrid FSO/RF scheme, which applies hardware switching between FSO and MMW RF links [11]. Another approach is to use both FSO and RF links for data transmission the whole time. One option in this approach is to transmit identical data simultaneously on both links and apply diversity combining techniques to received signals from both links [10], [22]. In this way, the system's data rate is limited to the lower rate of the RF link. Alternatively, the coded data stream is divided between the two links, which may have a significant improvement on total system capacity [23]. In general, this soft-switching approach requires FSO and RF links to be active continuously, even when FSO link has very good quality and can support the required bit-error rate by itself. In this scenario, RF transmission power is wasted and the system generates unnecessary RF interference to the environment [3].

## 2.3 Point-to-Multi-Point Transmission

The interesting and unique features of FSO systems motivated a wide range of interest in hybrid FSO/RF systems, as discussed in the last section. But most of the current literature is limited to point-to-point data transmissions with FSO technology. However, FSO can be used effectively in multiuser scenarios [5], [14] to support Point-to-Multi-Point (P2MP) topologies. The P2MP topology is a common network architecture for outdoor wireless networks to connect multiple locations to one single central location, as shown in Fig. 2.5.

In these P2MP networks, FSO links are used for data transmission from a central location to multiple users as in Wireless Internet Service Provider (WISP) networks. In a WISP network, subscribers are connected at the edge of the network using a client device typically mounted on the roof of their houses. The central base station is mounted on a high building where it has line of sight with the client devices.

Motivated by the scarcity of literature in this field, we propose a P2MP hybrid FSO/RF network. The proposed data transmission network consists of a number of remote nodes along with a central node. Each remote node in the network is connected to the central node via a separate primary FSO link. A common backup RF link is shared among all the remote nodes. Using a common RF channel will

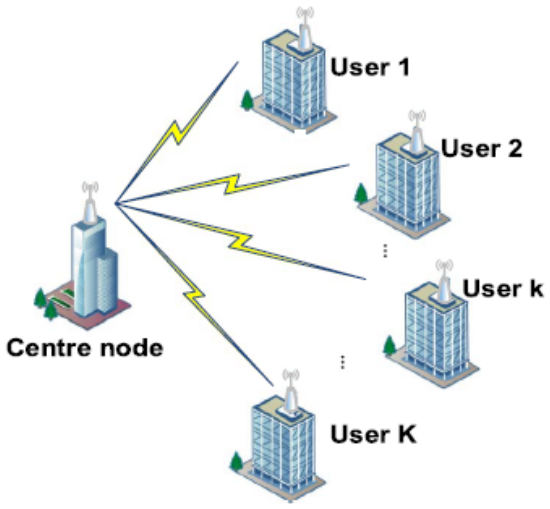


Figure 2.5: Diagram showing the point-to-multipoint FSO system [5]

.

have the major advantages of: 1) sharing the scarce RF spectrum, 2) preventing the generation of unnecessary RF interference to the environment, and 3) conserving the RF transmission power. In the next chapter, we discuss our proposed network in detail.

## 2.4 Summary

In this chapter, we have discussed FSO technology background and its application in the real world. Further, we have elaborated FSO - P2P technology and its applications. We discussed the shortcomings of FSO and defined Hybrid FSO/RF as an attractive alternative solution. Lastly, we discussed our thesis work that is on Hybrid P2MP FSO/RF systems. The next chapter describes our Hybrid P2MP FSO/RF network in detail with its performance metrics.

# Chapter 3

# Analysis of Point-to-Multi-Point Hybrid FSO/RF Network

In this chapter, we analyze a P2MP hybrid FSO/RF data transmission network, which consists of a number of remote nodes along with a central node. Each remote node in the network is connected to the central node via a primary FSO link. A common backup RF link is shared among all the remote nodes, where we adopt the simple switch-over hybrid FSO/RF approach. Using a common RF channel will have the major advantages of: 1) sharing the scarce RF spectrum, 2) preventing the generation of unnecessary RF interference to the environment, and 3) conserving the RF power. We study the performance of transmit buffers in the central node for each individual remote node by developing a Markovian chain model, with non-equal priority protocol and $p$-persistent strategy. Using this model, we study the throughput, the average buffer size, the frame queuing delay in the transmit buffer, the efficiency of the queuing system, and the frame loss probability are determined for the proposed FSO/RF topology.

## 3.1 P2MP Hybrid FSO/RF Network Modeling

The general block diagram of a P2MP hybrid FSO/RF network is shown in Fig. 3.1. This network consists of an central node and $N$ remote nodes. The central node is equipped with $N$ optical transmitters and one RF transmitter. Each remote node in the network is equipped with one optical receiver and one RF receiver. Each remote node of the network is connected to the central node through a separate primary

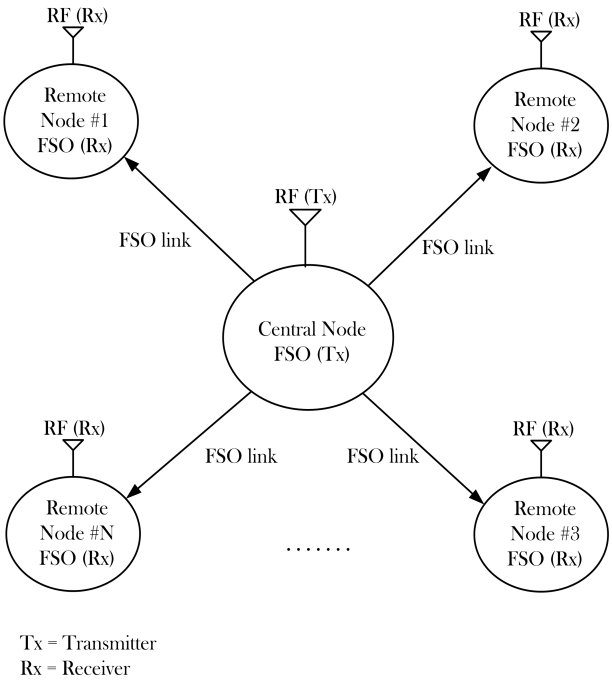


Figure 3.1: General block diagram of a P2MP Hybrid FSO/RF network.

.

FSO link. The central node is assumed to be aware of the quality of the $N$ FSO links through $N$ feedback channels. The RF transmitter of the central node is assigned a certain RF channel, which is used as a backup channel for data transmission to any remote node in case of the failure of its corresponding FSO link.

Through out the chapter, we will adopt the following assumptions:

1. The FSO channel is assumed to be constant during one data frame.
2. Simultaneous data transmission over FSO and RF links is not allowed.
3. All FSO channels and the backup RF channel are impaired by fading.
4. When more than one FSO link fails, the central node will use the RF link to communicate with one of the corresponding remote nodes on non-equal priority basis, where the lowest number node will have the highest priority.
5. Non-preemptive RF transmission is assumed.
6. The data frame is transmitted over the FSO and RF links at different rates.
7. Once the data frame is being transmitted using RF channel, it is assumed that RF channel will remain healthy through out the frame transmission.

## 3.2 Fading Probability of Transmission Links

In this transmission scheme, only the FSO link is used for data transmission as long as the instantaneous signal-to-noise ratio (SNR) at the optical receiver of the remote node is above a certain threshold. As we have established in the last section, FSO channels are impaired by fading, which causes attenuation in the link and reduces the SNR. When SNR falls below the certain threshold, the central node uses the RF link for data transmission.

We define $a$ to be the probability that a certain FSO link is in poor quality due to fading. The actual calculations of $a$ are defined in [3]. In our thesis, we only use certain values of $a$ are used which representative of typical weather conditions to test our model.

Similarly, the RF link is also affected by fading as per our assumptions; we define $b$ to be the probability that the RF link is in poor quality due to fading and can not be used for data transmission. The actual calculations for $b$ are defined in [3]; we only use certain values of $b$ representing typical weather conditions to test the model.

## 3.3 Non-equal Priority Protocol

Since we assumed only one back up RF link, in the event of FSO link failure the central node uses the RF link to transmit a frame to a remote node using a non-equal priority protocol. Non-equal priority protocol means that the remote nodes have different priorities in being assigned the RF link. Node 1 is considered the highest-priority node and Node 2 is the next highest-priority node, etc. Node $N$ is the least-priority node. When two or more nodes have faded FSO links, the central node checks the status of the RF links to these nodes and assigns the RF link to the highest-priority node.

## 3.4 P-persistent Strategy

We use $p$-persistent access strategy when using the RF link. A remote node will be assigned the RF link under four conditions:

1. The FSO link is faded.
2. The RF link is not faded.
3. The remote node has the highest priority among all nodes needing the RF link.
4. The central node allocates the RF link to that node with probability $p$.

Other protocols that use this scheme include: $p$-persistent CSMA/CA, $p$-persistent CSMA/CD and IEEE 802.11 (WiFi) [24].

## 3.5 Data Rates over FSO and RF links

The central node assigns a first-in-first-out (FIFO) transmit buffer of size $B$ frames for every remote node. The data frame arrives at the transmit buffer at rate $R_{in}$ frames/second. The frame arrival rate $R_{in}$ is assumed to be the same for all of the $N$ transmit buffers. We define $R_{out}$ as the frame departure rate given by:

$$R_{out} = \begin{cases} R_{FSO}, & \text{When transmiting data over the FSO link} \\ R_{RF}, & \text{When transmiting data over the RF link} \end{cases} \tag{3.1}$$

where $R_{FSO}$ and $R_{RF}$ are, respectively, frame transmission rates over FSO and RF links. $R_{FSO}$ and $R_{RF}$ are related by:

$$R_{FSO} = \Omega R_{RF} \tag{3.2}$$

It is worth mentioning that $\Omega$ will be restricted to integer values.

## 3.6 Discrete-Time Markov Chain Model

Markov process is a stochastic process which satisfies the Markov property. In Markov process the value of the random variable at instant $n$ depends only on its immediate past value at instant $n-1$. The random variable defines a state of the system at any given instant $n$ [24]. If the state of a Markov process changes in discrete time, the Markov process is called a discrete-time Markov chain.

The number of frames stored in the transmit buffer represent the state of the buffer. The future state of the buffer depends only on its current state and the change from one state to another will occur at discrete time values corresponding to frame arrival and departure events. Thus, we can use a discrete-time Markov chain to model the states of the transmit buffer for each remote node.

The time step of the discrete-time Markov chain, denoted by $T$, is chosen to be the inverse of the maximum data transmission rate on the line, as [24]:

$$T = \frac{1}{R_{FSO}} = \frac{1}{\Omega R_{RF}} \tag{3.3}$$

In order to calculate the performance of each node, we use the Markov chain model. We present the derivations of link accessing probabilities by central node in below sections which are required to construct a Markov chain model.

## 3.7 Probability of Central Node Accessing FSO Link to a Node

Since all the remote nodes are identical, and each node is equipped with an FSO link, we define $P_{FSO}$ to be the probability of using the FSO link by the central node to any of the remote nodes, which is given by :

$$P_{FSO} = 1 - a \tag{3.4}$$

## 3.8 Markov Chain Analysis

For the RF link to be used for data transmission to a remote node, it should be in good quality given that the FSO link is in poor quality. Since there is only one back up RF link which can be accessed by the central node, we use a non-equal priority protocol in terms of access to the RF link for a remote node and the first node will have the highest priority.

### 3.8.1 Probability of Accessing RF Link to First Node

We define $r_1$ to be the probability of the central node assigning an RF link for the highest priority node, which is given by:

$$r_1 = a(1-b)p \tag{3.5}$$

where $a$ denotes probability that the FSO link is in poor condition and $(1-b)$ represents that the RF link is available and is not being used by any other remote node and $p$ represents the persistent probability.

### 3.8.2 Discrete-Time Markov Chain Model for the First Node

We define the probability of frame arrival $\omega$ as the probability that a frame arrives at the buffer within the time step $T$. Or in other words, $\omega$ is the probability that a time step $T$ has a frame.

Based on our choice for the time step $T$ in (3.3), the resulting Markov chain is a single-arrival, single-departure queue. Here, we assume that when a frame arrives, it could be serviced and leaves the buffer at the same time step using the FSO link or could go to the next state RF link with a lower data rate. The corresponding state transition diagram of the transmit buffer of the first node is shown in Fig. 3.2. We define $s_{i,j}^{(1)}$ for $0 \leq i \leq B$ and $0 \leq j \leq \Omega - 1$ to be the buffer states. Here, $i$ represents the number of frames stored in the buffer, $j$ represents the number of rows since the beginning of frame transmission over RF link and $B$ represents the buffer size.

In Fig. 3.2 the state transition probabilities are defined as following:

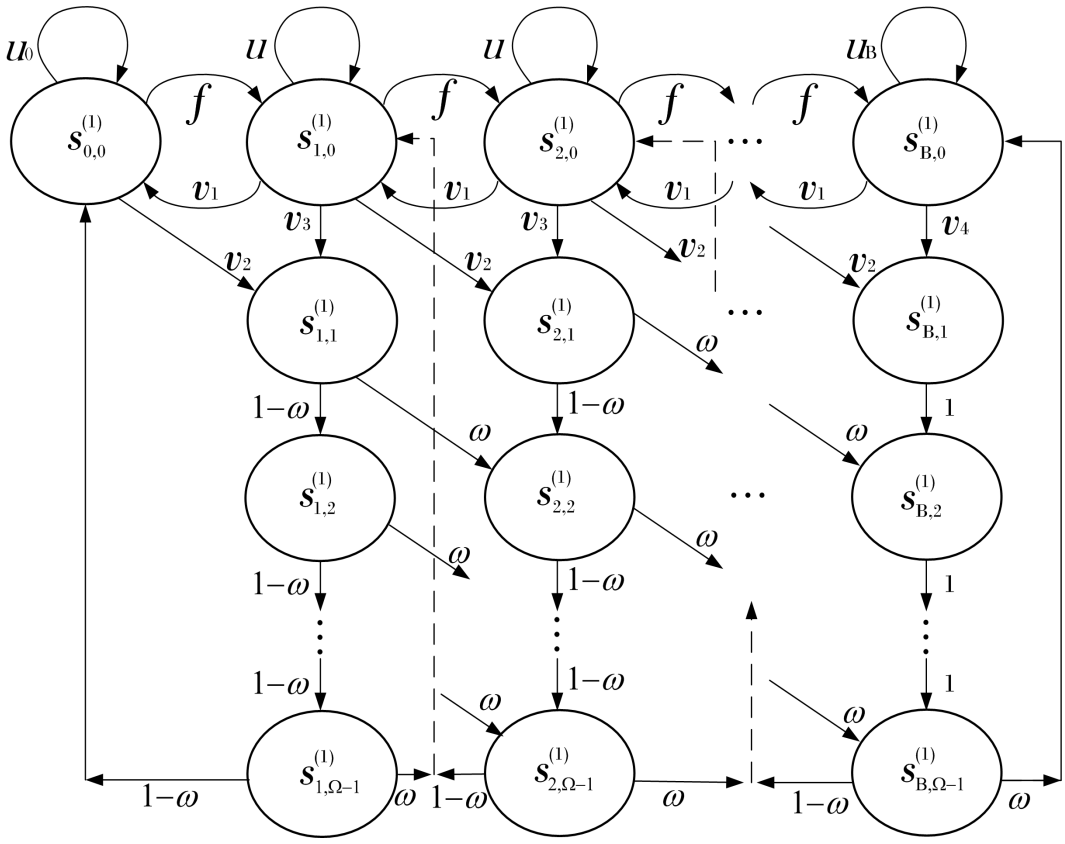


Figure 3.2: The state transition diagram for the transmit buffer of the first node.

$$
\begin{aligned}
u_0 &= 1-\omega+\omega P_{FSO},\\
f &= \omega[1-(P_{FSO}+r_1)] = \omega a(1-p)+\omega abp\\
u &= (1-\omega)[1-(P_{FSO}+r_1)]+\omega P_{FSO},\\
u_B &= 1-(P_{FSO}+r_1)+\omega P_{FSO},\\
\upsilon_1 &= (1-\omega)P_{FSO},\\
\upsilon_2 &= \omega r_1,\\
\upsilon_3 &= (1-\omega)r_1,\\
\upsilon_4 &= r_1.
\end{aligned}
\tag{3.6}
$$

The corresponding state transition matrix $P_1$ for the first node is given by:

$$
P_1 = \begin{bmatrix}
A_0 & C_0 & \phi_1 & \dots & \phi_1 & \phi_1 & \phi_1\\
E_0 & A & C & \dots & \phi_2 & \phi_2 & \phi_2\\
\phi_1^T & E & A & \dots & \phi_2 & \phi_2 & \phi_2\\
\phi_1^T & \phi_2 & E & \dots & \phi_2 & \phi_2 & \phi_2\\
\vdots & \vdots & \vdots & \ddots & \vdots & \vdots & \vdots\\
\phi_1^T & \phi_2 & \phi_2 & \dots & C & \phi_2 & \phi_2\\
\phi_1^T & \phi_2 & \phi_2 & \dots & A & C & \phi_2\\
\phi_1^T & \phi_2 & \phi_2 & \dots & E & A & C\\
\phi_1^T & \phi_2 & \phi_2 & \dots & \phi_2 & E & A_B
\end{bmatrix}_{\Omega B+1\times\Omega B+1}
\tag{3.7}
$$

where $A_0, C_0, E_0, A, C, E, A, A_B$, $\phi_1$, and $\phi_2$ are submatrices defined as:

$$
A_0 = \begin{bmatrix} u_0 \end{bmatrix}_{1\times 1}
\tag{3.8}
$$

$$
C_0 = \begin{bmatrix} \upsilon_1 & 0 & \dots & 0 & 1-\omega \end{bmatrix}_{1\times\Omega}
\tag{3.9}
$$

$$
E_0 = \begin{bmatrix} f & \upsilon_2 & 0 & \dots & 0 \end{bmatrix}^T_{1\times\Omega}
\tag{3.10}
$$

$$A = \begin{bmatrix} u & 0 & 0 & \dots & 0 & \omega \\ \upsilon_3 & 0 & 0 & \dots & 0 & 0 \\ 0 & 1-\omega & 0 & \dots & 0 & 0 \\ 0 & 0 & 1-\omega & \dots & 0 & 0 \\ \vdots & \vdots & \vdots & \ddots & \vdots & \vdots \\ 0 & 0 & 0 & \dots & 1-\omega & 0 \end{bmatrix}_{\Omega\times\Omega} \tag{3.11}$$

$$C = \begin{bmatrix} \upsilon_1 & 0 & 0 & \dots & 0 & 1-\omega \\ 0 & 0 & 0 & \dots & 0 & 0 \\ \vdots & \vdots & \vdots & \ddots & \vdots & \vdots \\ 0 & 0 & 0 & \dots & 0 & 0 \end{bmatrix}_{\Omega\times\Omega} \tag{3.12}$$

$$E = \begin{bmatrix} f & 0 & 0 & \dots & 0 & 0 \\ \upsilon_2 & 0 & 0 & \dots & 0 & 0 \\ 0 & \omega & 0 & \dots & 0 & 0 \\ 0 & 0 & \omega & \dots & 0 & 0 \\ \vdots & \vdots & \vdots & \ddots & \vdots & \vdots \\ 0 & 0 & 0 & \dots & \omega & 0 \end{bmatrix}_{\Omega\times\Omega} \tag{3.13}$$

$$A_B = \begin{bmatrix} u_B & 0 & 0 & \dots & 0 & \omega \\ \upsilon_4 & 0 & 0 & \dots & 0 & 0 \\ 0 & 1 & 0 & \dots & 0 & 0 \\ 0 & 0 & 1 & \dots & 0 & 0 \\ \vdots & \vdots & \vdots & \ddots & \vdots & \vdots \\ 0 & 0 & 0 & \dots & 1 & 0 \end{bmatrix}_{\Omega\times\Omega} \tag{3.14}$$

$$\phi_1 = \begin{bmatrix} 0 & 0 & 0 & \dots & 0 & 0 \end{bmatrix}_{1\times\Omega} \tag{3.15}$$

$$\phi_2 = \begin{bmatrix} 0 & 0 & 0 & \dots & 0 & 0 \\ 0 & 0 & 0 & \dots & 0 & 0 \\ \vdots & \vdots & \vdots & \ddots & \vdots & \vdots \\ 0 & 0 & 0 & \dots & 0 & 0 \end{bmatrix}_{\Omega\times\Omega} \tag{3.16}$$

The distribution vector $s^{(1)}$ corresponding to the state diagram in Fig. 3.2 and transition matrix (3.7) for the first remote node is given by:

$$
\begin{aligned}
s^{(1)} &= \begin{bmatrix} s_{0,0}^{(1)} & M_1 & M2 & ... & M_B \end{bmatrix}^T \\
M_k &= \begin{bmatrix} s_{k,0}^{(1)} & s_{k,1}^{(1)} & ... & s_{k,\Omega-1} \end{bmatrix}_{1\times\Omega} \\
& \qquad\qquad k = 1, 2, ...., B
\end{aligned} \tag{3.17}
$$

where $s_{i,j}^{(1)}$ for $0 \leq i \leq B$ and $0 \leq j \leq \Omega - 1$ represents the states of transmit buffer for first node.

At the steady state, the probability $s_{i,j}^{(1)}$ will not change with time. In this case, the distribution vector $s^{(1)}$ settles down to a unique value and satisfies the equation [24]:

$$P_1 s^{(1)} = s^{(1)} \tag{3.18}$$

This means that the steady state distribution vector $s^{(1)}$ is the eigenvector for $P_1$ corresponding to a eigenvalue that equals to one. MATLAB is for and other mathematical packages such as Maple and Mathematica have commands for finding that eigenvector. Having found a numeric answer, we must normalize $s^{(1)}$ to ensure that:

$$\sum_{i=0}^{B} \sum_{j=0}^{\Omega-1} s_{i,j}^{(1)} = 1 \tag{3.19}$$

### 3.8.3 Probability of Accessing RF Link to Second Remote Node

We define $r_2$ to be the probability of the central node using the RF link for the second node, and it is given by:

$$r_2 = a(1-b)\, p\, x_1 \tag{3.20}$$

where $a$ denotes the probability that the FSO link is in poor condition, $(1-b)$ represents that RF link is available, $p$ represents the probability by which a frame will be sent and $x_1$ is probability that the RF link is not being used by first remote node $x_1$, which is given as:

$$x_1 = 1 - y_1 \tag{3.21}$$

where in (3.21), $y_1$ is probability of first node accessing the RF link, defined by using the steady states of distribution vector $s^{(1)}$, which can be given as.

$$y_1 = (s_{0,0}^{(1)})\omega a(1-b)p + a(1-b)p\sum_{i=1}^{B}(s_{i,0}^{(1)}) + \sum_{i=1}^{B}\sum_{j=1}^{\Omega-1} s_{i,j}^{(1)} \tag{3.22}$$

where in (3.22) the first term on the RHS is the probability that a frame arrive for first node and leaves the system using RF link and the transmit buffer is empty.The second term and the third term on the RHS denotes the probability that a frame leaves the transmit buffer using RF link and the buffer is not empty.

### 3.8.4 Discrete-Time Markov Chain Model for the Second Node

The corresponding state transition diagram of the transmit buffer for the second node is similar to Fig. 3.2. We define $s_{i,j}^{(2)}$ for $0 \leq i \leq B$ and $0 \leq j \leq \Omega - 1$ to be the buffer states. Here, $i$ represents the number of frames stored in the buffer, $j$ represents the number of time steps elapsed since the beginning of frame transmission over RF link and $B$ represents the buffer size.

The state transition probabilities for second node are defined as following:

$$\begin{aligned}
u_0 &= 1 - \omega + \omega P_{FSO}, \\
f &= \omega[1 - (P_{FSO} + r_2)], \\
u &= (1-\omega)[1 - (P_{FSO} + r_2)] + \omega P_{FSO}, \\
u_B &= 1 - (P_{FSO} + r_2) + \omega P_{FSO}, \\
v_1 &= (1-\omega)P_{FSO}, \\
v_2 &= \omega r_2, \\
v_3 &= (1-\omega)r_2, \\
v_4 &= r_2
\end{aligned} \tag{3.23}$$

The state transition matrix $P_2$ for the corresponding state transition diagram will be same as shown in (3.7). Further, the steady state distribution vector $s^{(2)}$ corresponding to the state diagram of the second node in Fig. 3.2 is calculated using the same method as we used for the first node, which can be given as:

$$\begin{aligned} s^{(2)} &= \begin{bmatrix} s_{0,0}^{(2)} & M_1 & M2 & ... & M_B \end{bmatrix}^T \\ M_k &= \begin{bmatrix} s_{k,0}^{(2)} & s_{k,1}^{(2)} & ... & s_{k,\Omega-1} \end{bmatrix}_{1\times\Omega} \\ & \qquad\qquad k = 1, 2, ...., B \end{aligned} \tag{3.24}$$

### 3.8.5 Probability of Accessing RF Link to Third Remote Node

Similarly, we define $r_3$ to be the probability of using the RF link by the central node for the third node, which is given by:

$$r_3 = a(1-b)px_1x_2 \tag{3.25}$$

where $x_1$ and $x_2$ are the probabilities that RF link is not being used by central node for data transmission to the first and second node. $x_1$ is already defined previously in (3.21), $x_2$ can be given as:

$$x_2 = 1 - y_2 \tag{3.26}$$

where $y_2$ is probability of second node accessing the RF link, defined by using the steady states of distribution vector $s^{(2)}$, which can be given as:

$$y_2 = (s_{0,0}^{(2)})\omega a(1-b)p + a(1-b)p\sum_{i=1}^{B}(s_{i,0}^{(2)}) + \sum_{i=1}^{B}\sum_{j=1}^{\Omega-1} s_{i,j}^{(2)} \tag{3.27}$$

where the first term on the RHS is the probability that a frame arrives for second node and leaves the system using RF link and the transmit buffer is empty. The second and third term on the RHS denotes the probability that a frame leaves the transmit buffer using RF link and the buffer is not empty.

### 3.8.6 Generalize Equation for Non-equal Priority Protocol

To generalize the equation for $r_n$, where $n$ can be 1st, 2nd, 3rd ... $Nth$ remote node, the generalize equation can be given as:

$$r_n = a(1-b)p\prod_{j=0}^{n-1} x_j \tag{3.28}$$

where $1 \leq n \leq N$, $N$ is the total number of remote nodes and $x_0 = 1$.

## 3.9 Performance Metrics for a Node

The steady state distribution vector $s^{(n)}$ and RF link access probability $r_n$, allow us to analyse the various performance metrics for $n$ node as explained in the following subsections, where $n$ represents the number of the node ($1 \leq n \leq N$).

### 3.9.1 Throughput from Central Node to a Remote Node

We define the throughput $Th$ as the probability of successfully transmitting a frame over the FSO or RF link. Conditioning on the states of the transmit buffer for a node, $Th$ can be calculated as:

$$Th^{(n)} = \omega.s_{0,0}^{(n)}.(P_{FSO} + \frac{1}{\Omega}r_n) + (P_{FSO} + \frac{1}{\Omega}r_n)\sum_{i=1}^{B} s_{i,0}^{(n)} + \frac{1}{\Omega}\sum_{i=1}^{B}\sum_{j=1}^{\Omega-1} s_{i,j}^{(n)} \tag{3.29}$$

where $n$ represents the node number, the first term on the RHS is the probability that an arrived frame leaves the buffer when the buffer is empty. The second term on the RHS is the probability a frame leaves the buffer when it is not empty. The third term on the RHS is the probability that the rest of the frame is transmitted over the RF link. The $\frac{1}{\Omega}$ factor is because transmitting a frame over the back-up RF link requires $\Omega$ time steps. Or in other words, $\frac{1}{\Omega}$ of the frame is transmitted over RF link every time step.

### 3.9.2 Average Buffer Size

The average buffer size $Q_a$ is the average number of frames in the buffer, which can be expressed as:

$$Q_a{}^{(n)} = \sum_{i=1}^{B} \sum_{j=0}^{\Omega-1} i \; s_{i,j}^{(n)} \tag{3.30}$$

where $n$ represents the node number. The above expression represents the weighted sum of the number of frames in the buffer.

### 3.9.3 Average Buffer Queuing Delay

The average queuing delay $T_q$ is the average number of time steps that a frame spends in the buffer before being transmitted. Using Littles result, this delay is given by [24]:

$$T_q{}^{(n)} = \frac{Q_a{}^{(n)}}{Th^{(n)}} \tag{3.31}$$

where $n$ represents the node number.

### 3.9.4 Frame Loss Probability

A frame is lost when it arrives to a full transmit buffer and the frame at the head of the queue does not leave. Using traffic conversation principle described in [24] the frame loss probability $P_L$ can be given as following :

$$P_L{}^{(n)} = \omega - Th^{(n)} \tag{3.32}$$

where $n$ represents the node number.

### 3.9.5 Efficiency of the Queue

The efficiency of the queue $\varphi$ is defined as the ratio of probability of a frame leaving the buffer relative to the probability that a frame is arriving at the buffer. This can be expressed as:

$$\varphi^{(n)} = \frac{Th^{(n)}}{\omega} \tag{3.33}$$

where $n$ represents the node number.

The efficiency $\varphi$ gives an indication of frame loss due to buffer overflow. A value of $\varphi = 1$ implies no buffer overflow. A value of $\varphi < 1$ implies buffer overflow and potential frame loss.

## 3.10 Summary

In this chapter, we defined a P2MP network based on hybrid FSO/RF transmission system. A common backup RF link is used when the main FSO link is in poor condition. We studied performance of all nodes. A Markovian chain model was developed for transmit buffers of central node for all remote nodes considering different data rates of FSO and RF links and RF link to be accessed with non-equal priority and $p$-persistent strategy. We presented different performance matrices calculations such as throughput of the node, average transmit buffer size, queuing delay, efficiency of the queuing system and loss probability of frame. In the next chapter we present the simulation of network operation, the calculated performance matrices and summarize each result at the end.

# Chapter 4

# Analytical and Numeric Results

This chapter aims to present analytical and numerical results of the system described in Chapter 3. We developed a MATLAB code to study the performance evaluation of the defined network. In Section 4.1, we discuss the necessary relevant parameters for FSO and RF systems, and assumed values required to calculate performance of the network. In Section 4.2, we discuss Monte Carlo Simulation method and the algorithm used for numeric simulation. In Section 4.3, we discuss the graphs of different performance indices of the developed network and each graph is summarized at the end.

## 4.1 FSO and RF Link Probabilities

We evaluate our results using values of $a$ and $b$. Both the FSO and RF links are fading greatly affected by atmospheric conditions which are embedded in for the calculations of $a$ and $b$ in [3]. The FSO and RF links are affected by foggy and rainy weather, respectively. In our experiments as well, we consider values of $a$ for foggy weather conditions. We further consider values of $b$ for rainy weather conditions. Furthermore, in our experiments we consider different values of $p$-persistent and data rates for transmitting over RF link. Table 4.1 summarizes the parameter values we will use to evaluate the performance for our Hydrid FSO/RF system.

Table 4.1: Parameters of FSO and RF subsystems.

| FSO and RF subsystem | | |
|---|---|---|
| Parameter | Symbol | Value |
| Probability of FSO link in poor condition | $a$ | 0.99, 0.90 |
| Arrival probability | $\omega$ | 0.01 - 1.00 |
| Probability of RF link in poor condition | $b$ | 0.01, 0.20 |
| Total number of nodes | $N$ | 4 |
| Transmit buffer size | $B$ | 10 |
| p-persistent | $p$ | 0.25, 0.5, 1 |
| FSO to RF data rate | $\Omega$ | 1, 2 |

## 4.2 Numeric Simulation using Monte Carlo Method

Monte Carlo methods refer to a broad class of computational algorithms, that make use of repeated random number sampling to generate numerical results. This method is used to solve systems that might be deterministic in principle. We have developed a Matlab code as shown in Algorithm 4.1 to simulate Monte Carlo method to test our P2MP Hybrid FSO/RF model. Algorithm 4.1 follows the same Monte Carlo procedure as described in [25]. The simulation generates a large set of random possibilities, that are distributed over the simulation time ($T$). Algorithm 4.1 steps are defined as following:

1. Steps 1 and 2 defines the domain of input parameters.
2. Steps 3 and 5 generate random inputs distributed over the domain.
3. Steps 6 - 19 perform deterministic computations on the inputs.
4. Steps 20 - 24 calculate and aggregate the final results.

## 4.3 Results

### 4.3.1 Throughput ($Th$)

In Fig. 4.1, we consider $a = 0.99$, $b = 0.01$, $\Omega = 1$ in (3.2), which means the frame transmission rates of FSO and RF link are equal and the $p$-persistent value is considered as $p = 1$. It can be seen in Fig. 4.1(a) the throughput graph goes into

**Algorithm 4.1** Numerical Simualtion Pseudo code

```
Input: a, b, N, Ω, p, T, B, ω_min, ω_max
L ← 0(Node buffer)
Generate random channel states over time domain T
for ω_min to ω_max do
  Generate random symbols over time domain T,
  for t=1 to T do
    for n=1 to N do
      if L > B then
        lost_flag=1
      else
        L + 1
      end if
      if L >0 and FSO is good then
        Transmit_Symbol
      end if
      if L >0, RF is good , FSO is poor and RF≠1 then
        Transmit_Symbol
        RF ← 1
      end if
      Calculate Throughput
      Calculate Average buffer size
      Calculate Average delay
      Calculate Packet loss
      Calculate Efficiency
    end for
  end for
end for
```

three phases viz linear, dip and saturation. During the linear phase, a frame arrives and leaves the buffer immediately. This means that in this phase the buffer remains empty. For Node 1, the throughput is entirely linear for all frame arrival probabilities. Nodes 2, 3 and 4 experience sudden drops in throughput after the linear phase; the transition occurs when the transmit buffer is not empty and arriving frames can not leave the buffer because access to the RF link is restricted. As we have used a non-equal priority protocol, Node 1 has highest priority to access the RF link and priority decreases with increase in node number or access to the RF link for a node is restricted by a buffer of lower number node, which causes the drop in throughput for Nodes 2, 3 and 4. The throughput goes to saturation phase at $Th = 0$ for Node 3 and 4 because of having no access to RF link and no frame leaves the buffer. Fig. 4.1(b) shows

Monte Carlo simulation for the same parameters and results shows strong agreement with the analytical model.

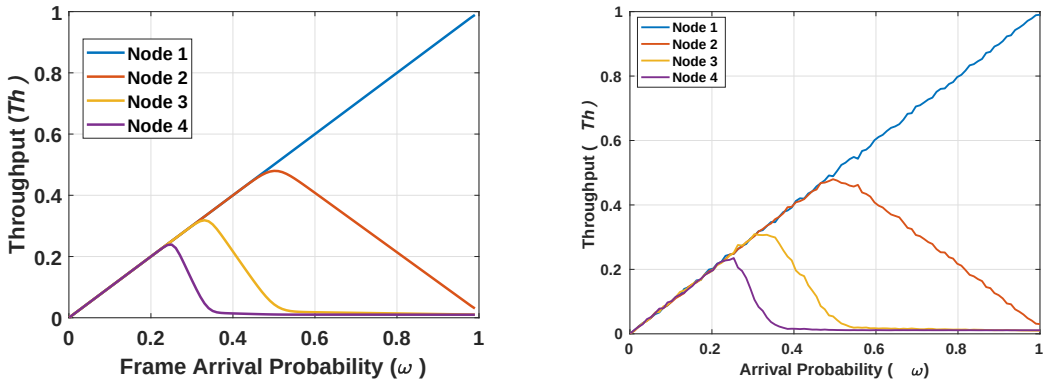


(a) (b)

Figure 4.1: Throughput with $a = 0.99$, $b = 0.01$, $\Omega = 1$, $p = 1$ and $B = 10$ symbols. (a) Analytical simulation. (b) Numeric simulation.

In Fig. 4.2, we consider the same values of $a$, $b$ and $\Omega$ as in Fig. 4.1. The $p$-persistent value is considered as $p = 0.50$, which means that even when the RF link is available, the probability of accessing the RF link for every node is 50%. It can be seen in Fig. 4.2 the throughput graph goes into three phases viz linear, saturation and dip. It is linear for small values of $\omega$. The saturation phase occurs for high values of $\omega$. For Node 1, the transition from linear to saturation phase occurs when the transmit buffer is not empty. The throughput for Node 1 saturates at $Th = 0.5$ because the RF link is being accessed with the probability $p$ and there is no dip in throughput. The Nodes 2, 3 and 4 experience sudden drops in throughput after the linear phase then reaches saturation. The drop is because of non-equal priority protocol. The throughput for Nodes 2, 3 and 4 saturates at $Th \neq 0$ because of $p$-persistent strategy; all remote nodes will have a chance to be assigned with RF link and to transmit frame over RF link, when the nodes of lower number are not transmitting over RF link.

In Fig. 4.3, we consider the same values of $a$, $b$, $\Omega$ as in Fig. 4.1 and value $p$-persistent is $p = 0.25$. The throughput of Node 1 buffer goes from linear to saturation phase when the buffer is not empty at $\omega = 0.25$ and settles at $Th = 0.25$ because of probability $p$, which is approximately half the value of the corresponding transition and saturation point at $\omega = 0.5$ and $Th = 0.5$ in Fig. 4.2 respectively. Nodes 2, 3 and 4 follows the similar trend as discussed in Fig. 4.1.

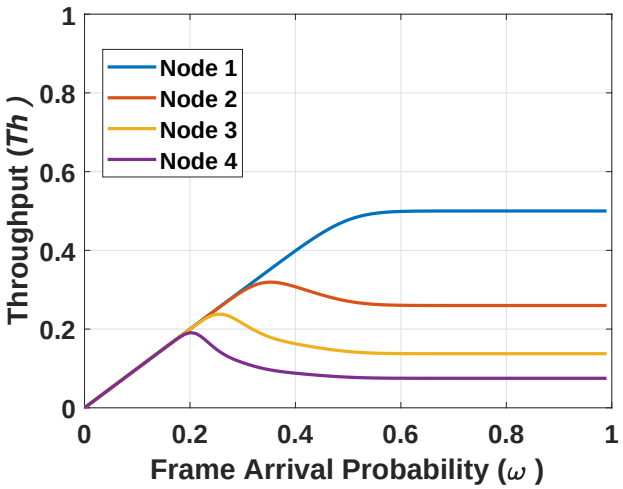


Figure 4.2: Throughput $a = 0.99$, $b = 0.01$, $\Omega = 1$, $p = 0.50$ and $B = 10$ symbols.

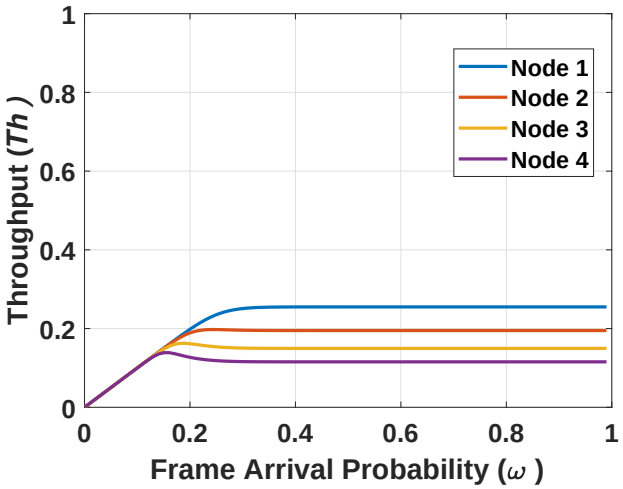


Figure 4.3: Throughput $a$=0.99, $b$=0.01, $\Omega = 1$, $p = 0.25$ and $B$= 10 symbols.

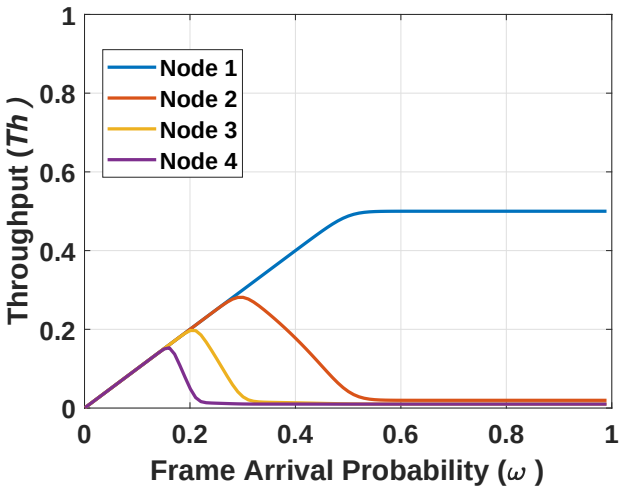


Figure 4.4: Throughput with $a = 0.99$, $b = 0.01$, $\Omega = 2$, $p = 1$ and $B = 10$ symbols.

In Fig. 4.4 we consider the same values of $a$, $b$ and $p$ as in Fig. 4.1 but $\Omega = 2$. It can be seen in Fig. 4.4, the throughput for Node 1 goes from linear to saturation phase at $\omega = 0.5$ because at the lower frame transmission rate of the RF link ($\frac{1}{2}$ of FSO link). Node 2 saturates at $\omega \simeq 0.57$ because of the RF link being used for Node 1 and Nodes 2, 3 and 4 follow the similar trend as discussed in Fig. 4.1.

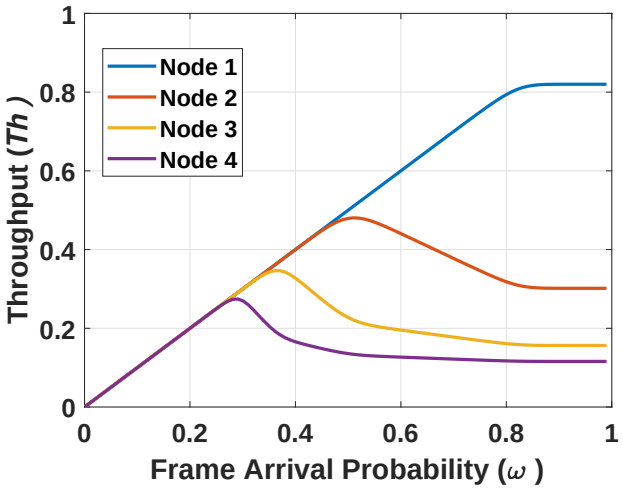


Figure 4.5: Throughput with $a = 0.90$, $b = 0.20$, $\Omega = 1$, $p = 1$ and $B = 10$ symbols.

In Fig. 4.5, we consider $a = 0.90$ and $b = 0.20$ with $\Omega = 1$ and $p = 1$. It can be seen in Fig. 4.5, For Node 1 buffer, the transition from linear to saturation phase occurs when the transmit buffer is not empty. The throughput for Node 1 saturates at $Th = 0.8$ because the RF link is 80% in good quality and there is no dip in throughput. The buffers for Nodes 2, 3 and 4 experience sudden drops in throughput after the linear phase because of non-equal priority protocol; the throughput for buffers then reaches saturation mode at the higher values of $\omega$ with probability FSO and available RF link.

It is of note that numerical simulations have shown that reducing the buffer size $B$ results in smoother transitions between the linear and the saturation phases of the throughput. The buffer size $B$ has no impact on the saturation values.

In this section we evaluated that under foggy weather conditions and no rain the transition point in throughput occurs at lower values of $\omega$ for higher values of $p$-persistent and $\Omega$. The throughput for Node 1 decreases with the high values of $p$-persistent probability and the chances for accessing RF link for the remaining nodes increase.

### 4.3.2 Average Buffer Size ($Q_a$)

We plot the average buffer size $Q_a$ as function of the frame arrival probability $\omega$ for different numbers of network nodes. The buffer size $B$ is considered 10 for all experiments. In Fig. 4.6, we consider $a = 0.99$, $b = 0.01$, $\Omega = 1$ in (3.2) and $p = 1$. It can be seen in Fig. 4.6(a) the $Q_a$ graph for Node 1, the buffer starts filling at high values $\omega$. This is because Node 1 has the highest priority to access the RF link, frames leave the buffer early upon arrival. Node 4 buffer starts filling at low values of $\omega$ because of having the lowest priority to access RF link. The average buffer size increases with smaller values of $\omega$ as the node numbers increase. The average buffer size $Q_a$ saturates at the maximum buffer size $B$ as expected. Fig. 4.6(b) shows Monte Carlo simulation for the same parameters. The strong similarities between the analytical and numeric results prove our analytical model to be accurate.

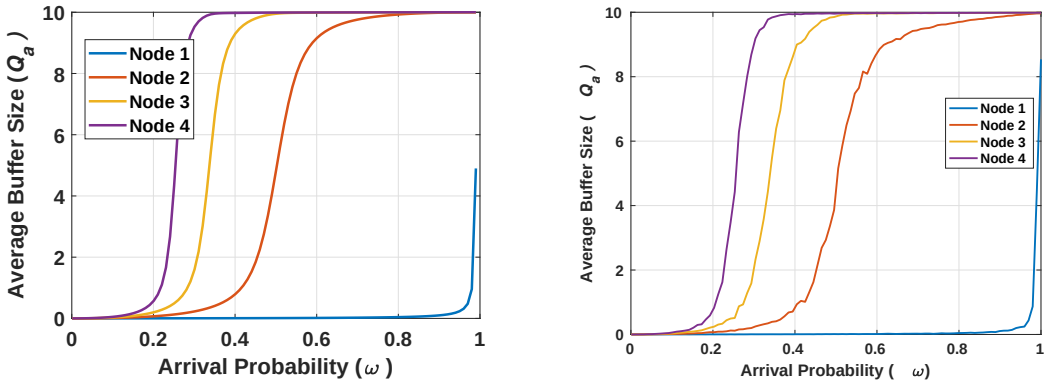


(a) (b)

Figure 4.6: Average buffer size with $a = 0.99$, $b = 0.01$, $\Omega = 1$, $p = 1$ and $B = 10$ symbols. (a) Analytical simulation. (b) Numeric simulation.

In Fig. 4.7, we consider $p = 0.50$ with same values of $a$, $b$ and $\Omega$ as in Fig 4.6. It can be seen in Fig. 4.7 that the Node 1 buffer starts filling approximately at $\omega = 0.4$. This is because of the persistent probability for accessing the RF link. Nodes 2, 3 and 4 follow similar trend as discussed in Fig. 4.11(a).

In Fig. 4.8, we consider $p = 0.25$ with same values of $a$, $b$ and $\Omega$ as in Fig 4.6. It can be seen in Fig. 4.8 the Node 1 buffer starts filling at very small value of $\omega$. This is because the low persistent probability for accessing the RF link. Nodes 2, 3 and 4 follow similar trend as discussed in Fig. 4.6(a).

In Fig. 4.9, we consider $\Omega = 2$ with same values of $a$, $b$ and $p$ as in Fig 4.6. It can

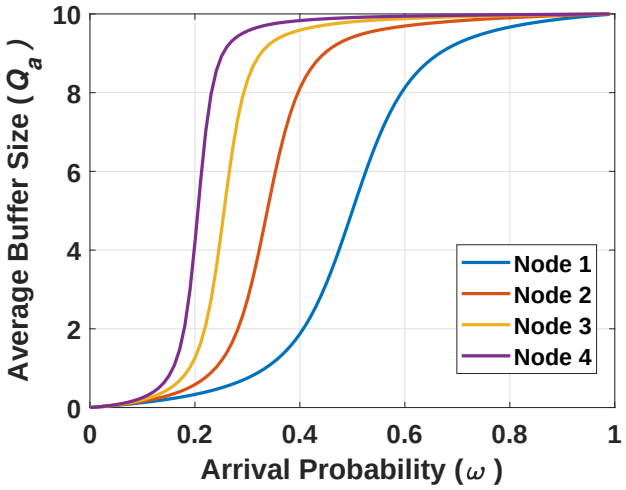


Figure 4.7: Average buffer size with $a = 0.99$, $b = 0.01$, $\Omega = 1$, $p = 0.50$ and $B = 10$ symbols.

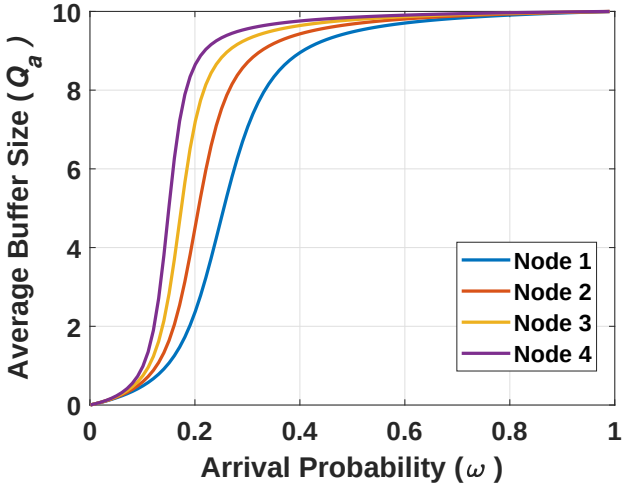


Figure 4.8: Average buffer size with $a = 0.99$, $b = 0.01$, $\Omega = 1$, $p = 0.25$ and $B = 10$ symbols.

be seen in Fig. 4.9 that the Node 1 buffer starts filling approximately at $\omega$=0.2. This is because the frame transmission rate of RF is half of the FSO link. Further, there is a minimal change observed in $Q_a$ when we change $\Omega$ to 1 and 2 for all the nodes.

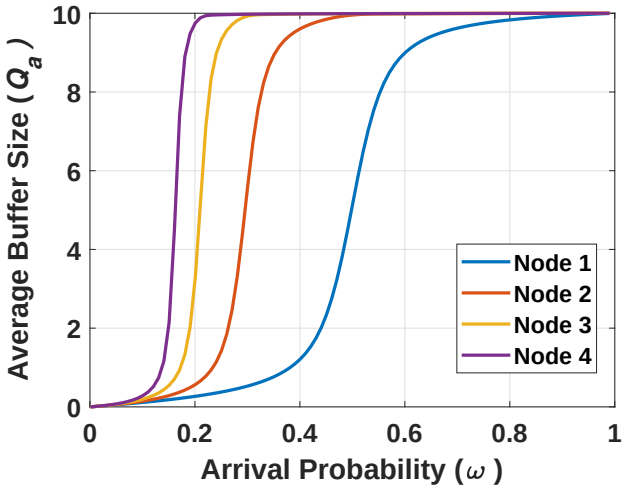


Figure 4.9: Average buffer size with $a$=0.99, $b$=0.01, $\Omega = 2$, $p$=1, and $B$= 10 symbols.

In Fig. 4.10, we consider $a = 0.90$, $b = 0.20$ with $\Omega = 1$ and $p = 1$. It can be seen in Fig. 4.10 buffer start filling at $\omega = 0.8$ for Nodes 1. This is because RF link is in 20% poor condition as compared to Node 1 in Fig. 4.6(a). Nodes 2, 3 and 4 follow similar trend as discussed in Fig. 4.11(a).

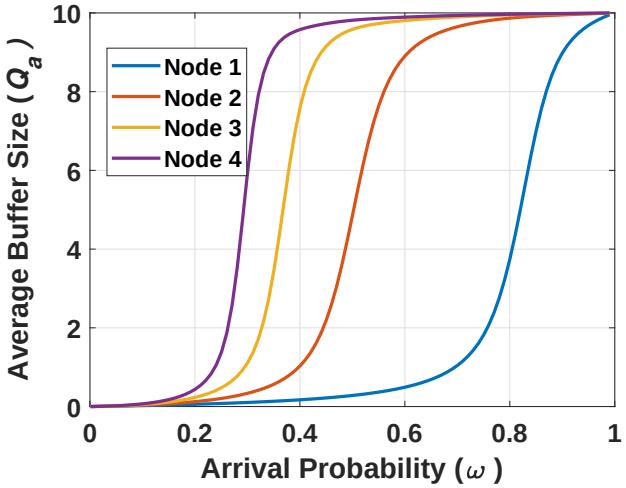


Figure 4.10: Average buffer size with $a = 0.90$, $b = 0.20$, $\Omega = 1$, $p = 1$, and $B = 10$ symbols.

In this section we evaluated that under foggy weather conditions and no rain, the

transmit buffer for all nodes starts filling at lower values of $\omega$ for higher values of $\Omega$ and $p$-persistent probability.

### 4.3.3 Average Queuing Delay ($T_q$)

We plot the Average queuing delay ($T_q$) as function of the frame arrival probability $\omega$ for different values of $N$. The buffer size $B$ is considered 10 for all experiments. The average queuing delay starts at low values then starts increasing after a certain frame arrival probability value $\omega$. The delay increases with increasing number of nodes and traffic ($\omega$). In Fig. 4.11(a), we consider $a = 0.99$, $b = 0.01$, $\Omega = 1$ in (3.2) and $p = 1$. The best performance occurs for the case of Node 1 because of having highest priority to access backup RF link. The worst performance occurs for Node 4 because of having the lowest access to RF link. The access to the RF link for a node is restricted by a node of lower number, which causes the performance to decrease (high values of Average buffer delay for small of values $\omega$). Fig. 4.11(b) shows Monte Carlo simulation for the same parameters. The numerical results strongly coincide with analytical results, proving our analytical model to be accurate.

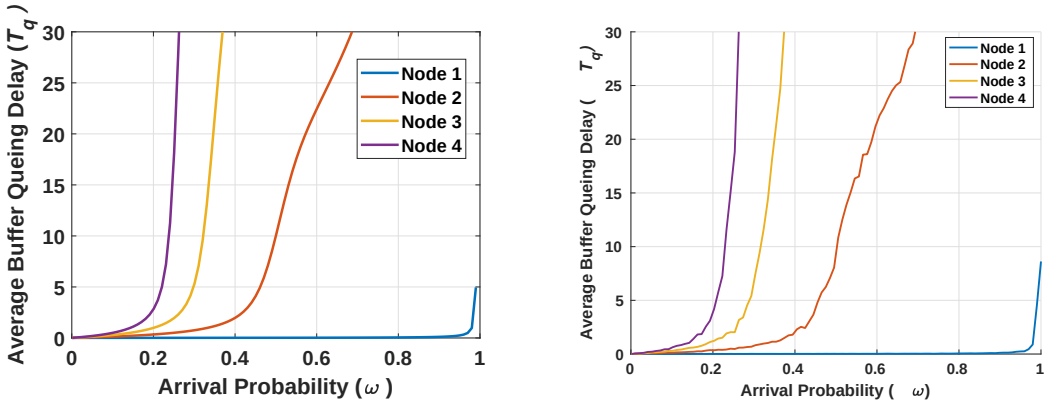


Figure 4.11: Average buffer delay with $a = 0.99$, $b = 0.01$, $\Omega = 1$, $p = 1$ and $B = 10$ symbols. (a) Analytical simulation. (b) Numeric simulation.

In Fig. 4.12, we consider $a = 0.99$, $b = 0.01$, $\Omega = 1$ and $p = 0.5$. It can be seen in Fig. 4.12, for Node 1 the value of Average buffer delay starts increasing at $\omega = 0.3$ and the $T_q \neq 0$ for all the nodes; this is because of the $p$-persistent probability, every incoming frame will spend some time in the buffer before being transmitted.

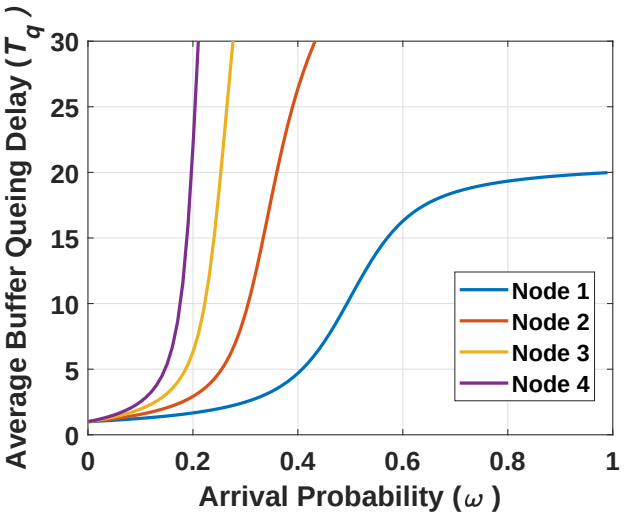


Figure 4.12: Average buffer delay with $a = 0.99$, $b = 0.01$, $\Omega = 1$, $p = 0.50$ and $B = 10$ symbols.

In Fig. 4.13, we consider $a = 0.99$, $b = 0.01$, $\Omega = 1$ in (3.2) and $p = 0.25$. It can be seen in Fig. 4.13, for all nodes Average buffer delay is not equal to zero at very low value of $\omega$ and higher than corresponding point in Fig. 4.12; this is because of the high value of the $p$-persistent probability. The frame will wait longer in the buffer as persistent strategy resist a frame from being transmitted. Node 1, Average buffer delay increases at small value of $\omega$ because of having low access to RF link (as determined by $p$-persistent strategy).

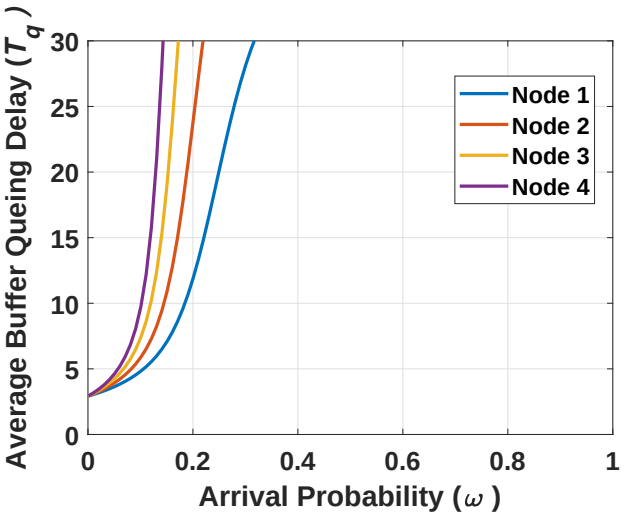


Figure 4.13: Average buffer delay with $a = 0.99$, $b = 0.01$, $\Omega = 1$, $p = 0.25$ and $B = 10$ symbols.

In Fig. 4.14, we consider the same values of $a$, $b$ and $p$ as in Fig. 4.11 with $\Omega = 2$. It can be seen in Fig. 4.14, the value of Average buffer delay for Node 1 starts increasing approximately at $\omega = 0.45$. This is because frame transmission rate of RF link is half of FSO link. The average buffer queuing delay starts increasing at lower values $\omega$ for Nodes 2, 3 and 4 as compared to Fig. 4.11(a). This is because the RF access is minimal for all nodes. Further, there is a minimal change observed in the Average buffer delay when we change $\Omega$ from 1 to 2 for all the nodes.

In Fig. 4.15, we consider $a = 0.90$, $b = 0.20$ with $\Omega = 1$ and $p = 1$. It can be seen in Fig. 4.15, Average buffer delay for Node 1 starts increasing at $\omega = 0.8$, this is because RF link is in 20% poor condition as compared to Fig. 4.11(a). Nodes 2, 3 and 4 follow similar trend as defined previously in Fig. 4.11(a) because of having access restrictions to the RF link.

In this section we evaluated that under foggy weather conditions and no rain the Average buffer queuing delay starts increasing at lower values of $\omega$ for higher values

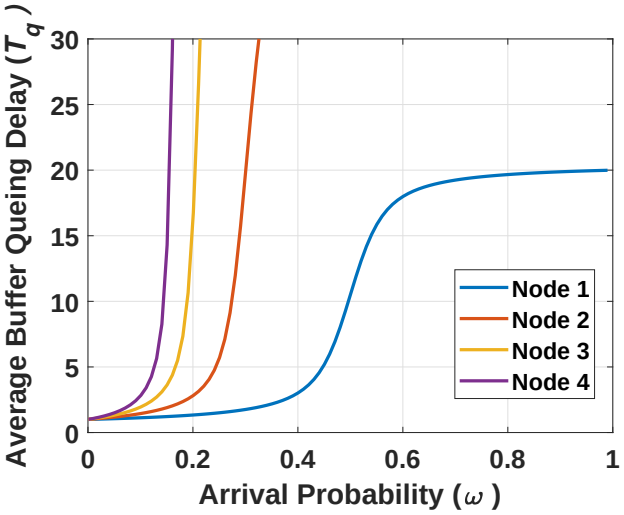


Figure 4.14: Average buffer delay with $a = 0.99$, $b = 0.01$, $\Omega = 2$, $p = 1$ and $B = 10$ symbols.

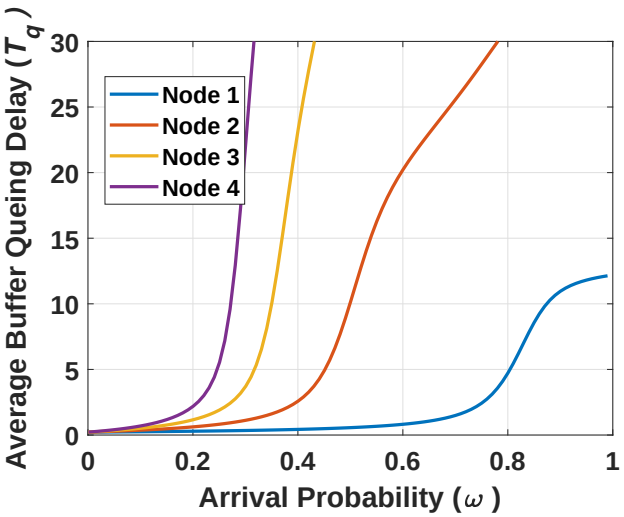


Figure 4.15: Average buffer delay with $a = 0.90$, $b = 0.20$, $\Omega = 1$, $p = 1$, and $B = 10$ symbols.

of $\Omega$ and $p$-persistent probability, as incoming traffic increases buffer queuing delay also increases for all the nodes.

### 4.3.4 Frame Loss Probability( $P_L$ )

We plot the frame loss probability ($P_L$) against the frame arrival probability $\omega$. We consider buffer size ($B$) as 10 in all experiments. The loss probability goes into two phases zero loss and viz linear. The zero loss phase occurs at low values of $\omega$. The linear phase occurs at higher values of $\omega$. The transition point occur when the buffer is full. In Fig. 4.16(a), we consider $a = 0.99$, $b = 0.01$, $\Omega = 1$ in (3.2) and $p = 1$. It can be seen in Fig. 4.16(a) that Node 1 shows zero loss. This is because Node 1 has the highest priority to access the RF link and to transmit the frame, hence the buffer never gets full. The Nodes 2, 3 and 4 transition points occur at lower values of $\omega$. This is because the RF link access priority decreases with increase in node number and the buffer starts filling up at lower value of $\omega$. Fig. 4.16(b) shows Monte Carlo simulation for the same parameters. The strong similarities between the analytical and numeric results prove our model to be accurate.

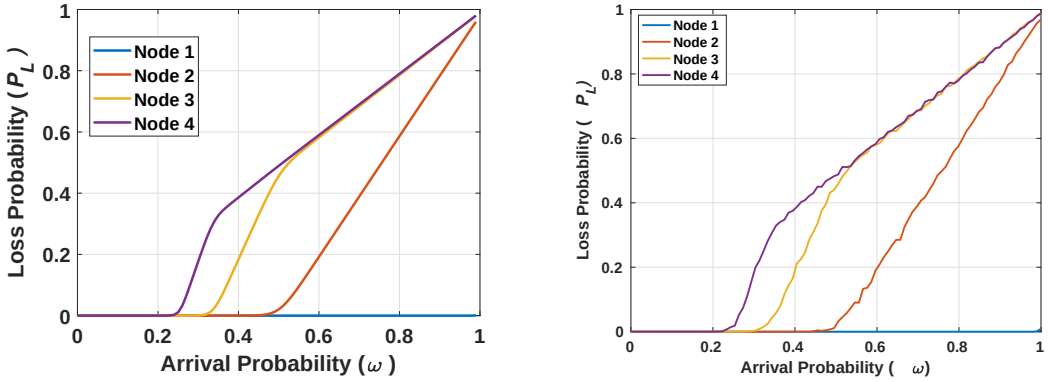


(a) (b)

Figure 4.16: Loss probability with $a = 0.99$, $b = 0.01$, $\Omega = 1$, $p = 1$ and $B = 10$ symbols. (a) Analytical simulation. (b) Numeric simulation.

In Fig. 4.17, we consider the same values of $a$, $b$, $\Omega$ as in Fig. 4.16 with $p = 0.50$. The loss probability of Node 1 goes from zero to linear phase at $\omega = 0.5$, which is approximately half the value of the corresponding graph for Node 1 in Fig. 4.16(a). This is because persistent probability $p = 0.50$, which stops a frame from being transmitted and the buffer starts getting full at lower values of $\omega$ for all the nodes.

Nodes 2, 3 and 4 follow similar trend as defined in in Fig. 4.16(a), with slightly less loss probability.

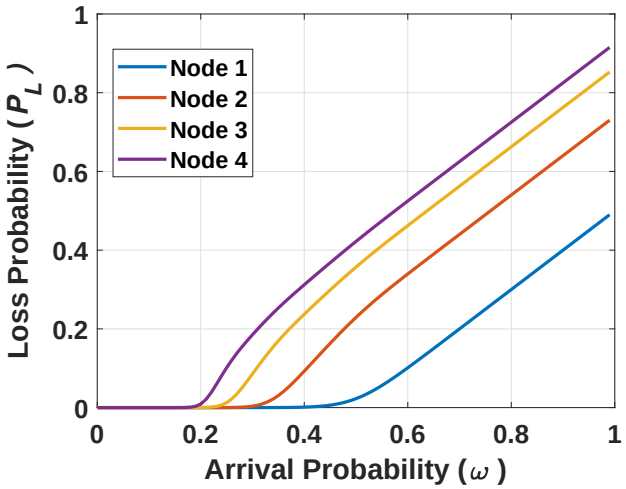


Figure 4.17: Loss probability with $a = 0.99$, $b = 0.01$, $\Omega = 1$, $p = 0.50$ and $B = 10$ symbols.

Similarly, in Fig. 4.18 we consider the same values for $a$, $b$, $\Omega$ as in Fig. 4.16 with $p = 0.25$. Loss probability transition point for Node 1 occurs at $\omega = 0.25$, this is because the persistent probability ($p = 0.25$), which stops a frame from being transmitted and the buffer starts getting full at lower values of $\omega$ for all nodes. Nodes 2, 3 and 4 follow similar trend as defined previously.

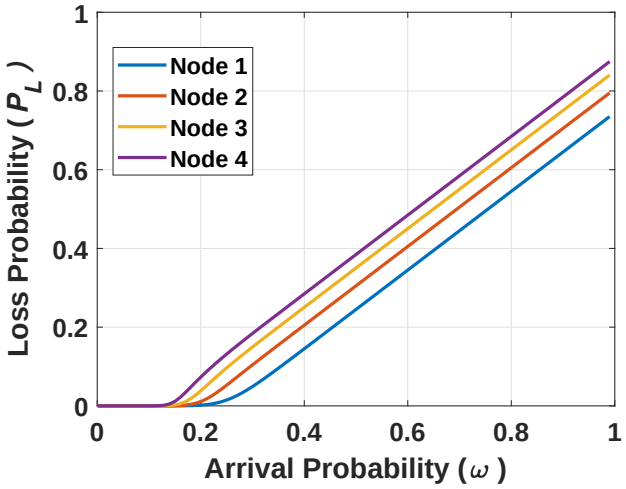


Figure 4.18: Loss probability with $a = 0.99$, $b = 0.01$, $\Omega = 1$, $p = 0.25$ and $B = 10$ symbols.

In Fig. 4.19, we consider the same values for $a$, $b$ as in Fig. 4.16 but with $\Omega = 2$ and $p = 1$. It can be seen in Fig. 4.19, for Node 1 the loss probability starts increasing at $\omega = 0.5$, which is approximately half the value of the corresponding graph in Fig. 4.16(a). This is because frame transmission rate of RF link is half of the FSO link. Nodes 2, 3 and 4 graph follows the similar trend as discussed in Fig. 4.16(a).

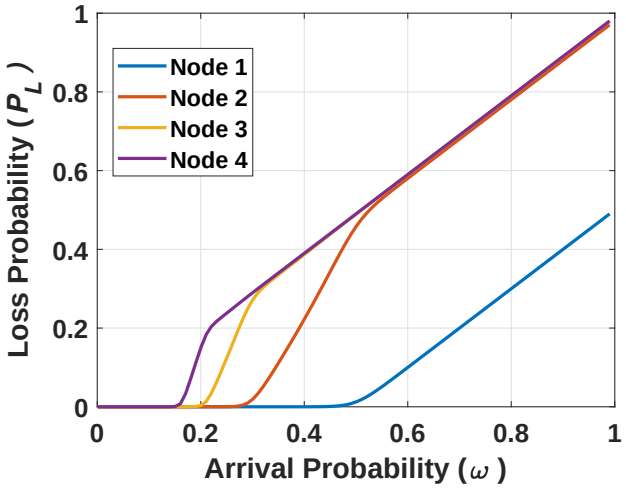


Figure 4.19: Loss probability with $a = 0.99$, $b = 0.01$, $\Omega = 2$, $p = 1$ and $B = 10$ symbols.

In Fig. 4.20, we consider $a = 0.90$, $b = 0.20$, $\Omega = 1$ and $p = 1$. It can be seen in Fig. 4.20, the transition point for Node 1 in loss probability($P_L$) occurs at $\omega = 0.8$, this is because the RF link is 20% in poor condition as compared to corresponding graph in Fig. 4.16(a). Nodes 2, 3 and 4 follow similar trend as discussed previously in Fig. 4.16(a).

In this section we evaluated that under foggy weather conditions and no rain the transition point in loss probability occurs at lower values of $\omega$ for higher values of $\Omega$ and $p$-persistent probability. As incoming traffic increases, loss probability also increases, subjected to availability of transmission links.

### 4.3.5 Efficiency ($\varphi$)

We plot the efficiency ($\varphi$) as function of the symbol arrival probability $\omega$ for different values of $N$. The efficiency ($\varphi$) goes into two phases viz unity efficiency and decreasing efficiency. The unity efficiency phase occurs at low $\omega$ values. The decreasing efficiency occurs for higher values of $\omega$. The transition point occurs when the buffer is not empty.

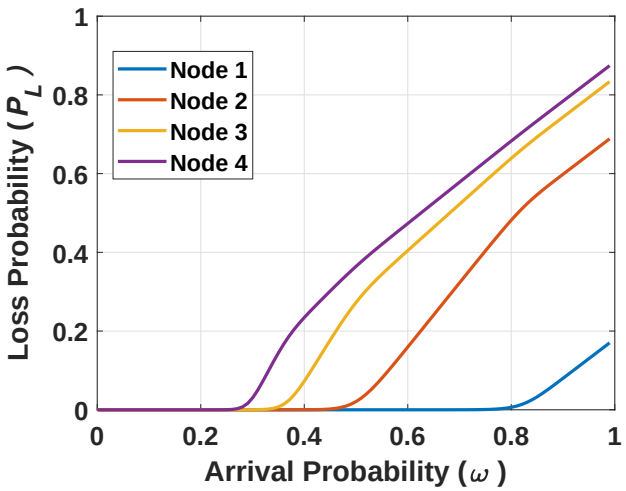


Figure 4.20: Loss probability with $a = 0.90$, $b = 0.20$, $\Omega = 1$, $p = 1$, and $B = 10$ symbols.

We consider buffer size ($B$) as 10 in all experiments.

In Fig. 4.21, we consider $a = 0.99$, $b = 0.01$, $\Omega = 1$ in (3.2) and $p = 1$. It can be seen in Fig. 4.21 the efficiency for Node 1 is always unity. This is because Node 1 has the highest priority to access RF link. The Nodes 2, 3 and 4 transition points in efficiency occur at lower values of $\omega$. This is because the RF link access priority decreases with increase in node number. The access to the RF link for a node is restricted by a node of lower number. Fig. 4.21(b) shows Monte Carlo simulation for the same parameters and results show strong agreement with the analytical model.

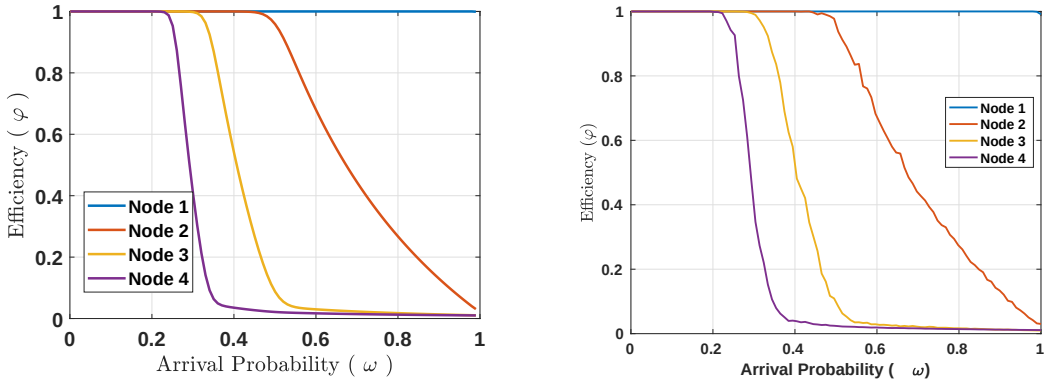


(a) (b)

Figure 4.21: Efficiency with $a = 0.99$, $b = 0.01$, $\Omega = 1$, $p = 1$ and $B = 10$ symbols. (a) Analytical simulation. (b) Numeric simulation.

In Fig. 4.22, we consider $a = 0.99$, $b = 0.01$, $\Omega = 1$ and $p = 0.50$, the efficiency of Node 1 goes from unity to decreasing efficiency at $\omega = 0.5$; this is because of persistent probability, which transmits frame with probability $p$, increasing the chances for a frame being transmitted to all the nodes. The efficiency for Nodes 2, 3 and 4 increased as compared to Fig. 4.21(a) because of persistent probability, and follows the similar trend as discussed in Fig. 4.21(a).

Similarly, in Fig. 4.23 we consider the same values of $a$, $b$, $\Omega$ as in Fig. 4.21 with $p = 0.25$. Node 1 efficiency transition point occur at $\omega = 0.25$, this is because of persistent strategy, a frame is being transmitted with $p = 0.25$. Nodes 2, 3 and 4 follows the similar trend as discussed in Fig. 4.21(a).

In Fig. 4.24, we consider the same values of $a$, $b$ as in Fig. 4.21 with $\Omega = 2$ in (3.2) and $p = 1$. It can be seen in Fig. 4.24, with $\Omega = 2$, efficiency for Node 1 goes from unity to decreasing efficiency at $\omega = 0.5$, which is approximately half the value to

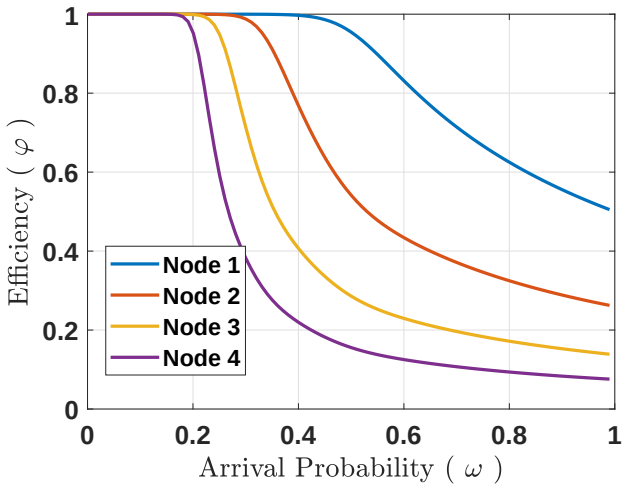


Figure 4.22: Efficiency with $a = 0.99$, $b = 0.01$, $\Omega = 1$, $p = 0.50$ and $B = 10$ symbols.

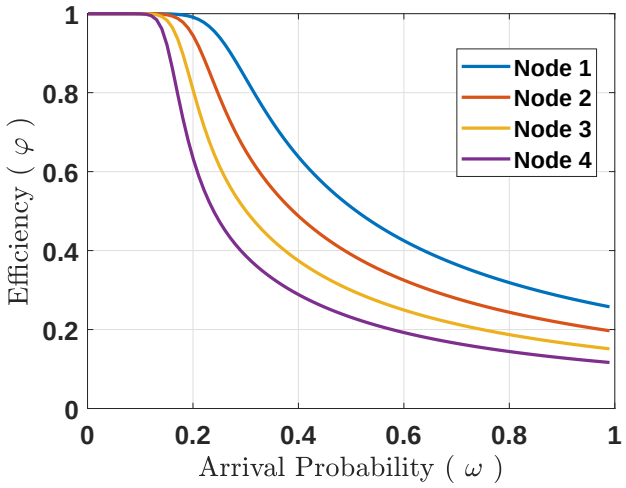


Figure 4.23: Efficiency with $a = 0.99$, $b = 0.01$, $\Omega = 1$, $p = 0.25$ and $B = 10$ symbols.

the corresponding graph in Fig. 4.21(a), this is because of lower frame transmission rate of the RF link (half of FSO link). Nodes 2, 3 and 4 follows the similar trend as discussed in Fig. 4.21(a).

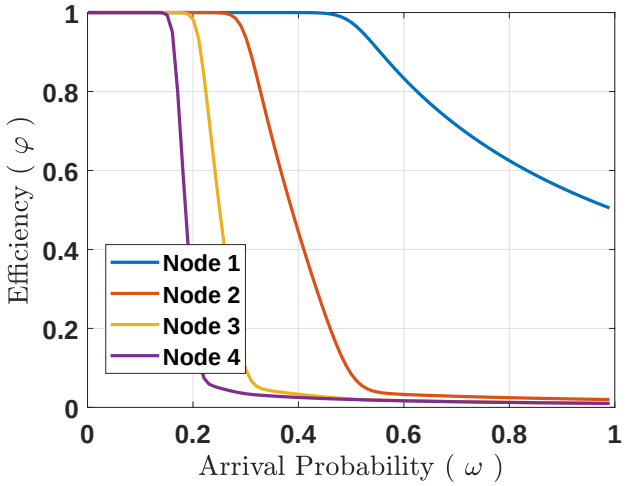


Figure 4.24: Efficiency with $a = 0.99$, $b = 0.01$, $\Omega = 2$, $p = 1$ and $B = 10$ symbols.

In Fig. 4.25, we consider $a = 0.90$ and $b = 0.20$. It can be seen in Fig. 4.25, the efficiency for Node 1 goes from unity to decreasing efficiency at $\omega = 0.8$, this is because the RF link is 20% poor condition as compared to in Fig. 4.21(a). Node 2, 3 and 4 follow similar trend as discussed in Fig. 4.21(a).

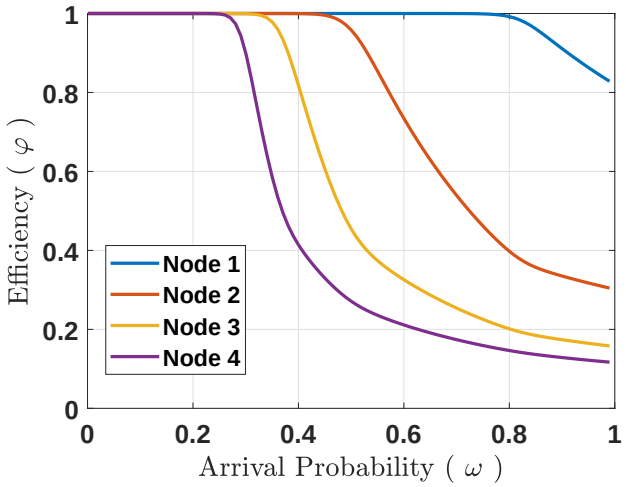


Figure 4.25: Efficiency with $a = 0.90$, $b = 0.20$, $\Omega = 1$, $p = 1$, and $B = 10$ symbols.

In this section we evaluated that under foggy weather conditions and no rain the

transition point in ($\varphi$) occurs at lower values of $\omega$ for higher values of $\Omega$ and persistent probability. As incoming traffic increases, efficiency decreases subject to availability of transmission links.

# Chapter 5

# Conclusions and Contributions

In this chapter, the accomplished work is summarized and contributions are highlighted.

## 5.1 Conclusion

The complementary nature of FSO and MMW RF links led to various approaches in developing hybrid FSO/RF data transmission systems. Considering a multi-user scenario, we proposed and analysed a P2MP Hybrid FSO/RF Network. In this network, a common backup RF link is used by the central node for data transmission to any remote node in case of the failure of its corresponding FSO link. We developed a discrete-time Markov chain model for the transmit buffer of the link between the central node and all the remote nodes. Studying each node allowed us to investigate several performance criteria such as throughput from central node to the remote node, the average transmit buffer size, the symbol queuing delay in the transmit buffer, the efficiency of the queuing system, and the symbol loss probability. Using a common backup RF link with non-equal equal priority protocol basis, $p$-persistent strategy and different data rates as compared to FSO link, our proposed P2MP Hybrid FSO/RF network can achieve considerable better performance under foggy and dry weather conditions. We presented a useful tool, which can be utilized by researchers implementing hybrid multi-user FSO/RF systems for real world applications and performance calculations.

## 5.2 Contributions

We have evaluated the performance of transmit buffers in hybrid P2MP FSO/RF systems, using analytical performance evaluation and proved our model with numeric simulation using Monte-Carlo method. The major contributions of this thesis are stated below.

1. A Markov chain model of the proposed network is developed for every individual remote node.

2. A non-equal priority protocol is proposed, when transmitting to a remote node using RF link, where Node 1 is considered highest priority.

3. An analytical model is developed to identify the main parameters of the system, we further verified our results using Monte Carlo method, proving our analytical model to be accurate.

# Bibliography

[1] E. Leitgeb, S. S. Muhammad, C. Chlestil, M. Gebhart, and U. Birnbacher, "Reliability of FSO links in next generation optical networks," in *Proceedings of 7th International Conference on Transparent Optical Networks*, vol. 1. IEEE, 2005, pp. 394–401.

[2] D. Schulz, V. Jungnickel, C. Alexakis, M. Schlosser, J. Hilt, A. Paraskevopoulos, L. Grobe, P. Farkas, and R. Freund, "Robust optical wireless link for the backhaul and fronthaul of small radio cells," *Journal of Lightwave Technology*, vol. 34, no. 6, pp. 1523–1532, 2016.

[3] T. Rakia, "Performance analysis of hybrid optical wireless and radio frequency communication systems," Ph.D. dissertation, University of Victoria, Victoria, BC, 2016.

[4] E. Zedini, A. Chelli, and M.-S. Alouini, "On the performance analysis of hybrid ARQ with incremental redundancy and with code combining over free-space optical channels with pointing errors," *IEEE Photonics Journal*, vol. 6, no. 4, pp. 1–18, 2014.

[5] P. Wang, N. Xiang, Q. Gao, R. Wang, L. Guo, and Y. Yang, "On the performances of $N$th best user selection scheme in multiuser diversity free-space optical systems over exponentiated weibull turbulence channels," *IEEE Photonics Journal*, vol. 8, no. 2, pp. 1–15, 2016.

[6] L. C. Andrews, R. L. Phillips, and C. Y. Hopen, *Laser beam scintillation with applications*. SPIE press, 2001, vol. 99.

[7] F. Giannetti, M. Luise, and R. Reggiannini, "Mobile and personal communications in the 60 GHz band: A survey," *Wireless Personal Communications*, vol. 10, no. 2, pp. 207–243, 1999.

[8] F. Nadeem, V. Kvicera, M. S. Awan, E. Leitgeb, S. S. Muhammad, and G. Kandus, "Weather effects on hybrid FSO/RF communication link," *IEEE Journal on Selected Areas in Communications*, vol. 27, no. 9, 2009.

[9] H. Wu and M. Kavehrad, "Availability evaluation of ground-to-air hybrid FSO/RF links," *International Journal of Wireless Information Networks*, vol. 14, no. 1, pp. 33–45, 2007.

[10] N. D. Chatzidiamantis, G. K. Karagiannidis, E. E. Kriezis, and M. Matthaiou, "Diversity combining in hybrid RF/FSO systems with PSK modulation," in *International Conference on Communications (ICC)*. IEEE, 2011, pp. 1–6.

[11] M. Usman, H.-C. Yang, and M.-S. Alouini, "Practical switching-based hybrid FSO/RF transmission and its performance analysis," *Photonics Journal*, vol. 6, no. 5, pp. 1–13, 2014.

[12] T. Rakia, H.-C. Yang, M.-S. Alouini, and F. Gebali, "Outage analysis of practical FSO/RF hybrid system with adaptive combining," *IEEE Communications Letters*, vol. 19, no. 8, pp. 1366–1369, 2015.

[13] T. Rakia, F. Gebali, H.-C. Yang, and M.-S. Alouini, "Cross layer analysis of P2MP hybrid FSO/RF network," *Journal of Optical Communications and Networking*, vol. 9, no. 3, pp. 234–243, 2017.

[14] S. Zhalehpour, M. Uysal, O. A. Dobre, and T. Ngatched, "Outage capacity and throughput analysis of multiuser FSO systems," in *14th Canadian Workshop on Information Theory (CWIT)*. IEEE, 2015, pp. 143–146.

[15] A. K. Majumdar and J. C. Ricklin, *Free-space laser communications: principles and advances*. Springer Science & Business Media, 2010, vol. 2.

[16] D. M. Boroson, B. S. Robinson, D. V. Murphy, D. A. Burianek, F. Khatri, J. M. Kovalik, Z. Sodnik, and D. M. Cornwell, "Overview and results of the lunar laser communication demonstration," in *Proc. SPIE*, vol. 8971, 2014, p. 89710S.

[17] J. R. Barry, J. M. Kahn, W. J. Krause, E. A. Lee, and D. G. Messerschmitt, "Simulation of multipath impulse response for indoor wireless optical channels," *Journal on selected areas in communications*, vol. 11, no. 3, pp. 367–379, 1993.

[18] A. T. Hussein, M. T. Alresheedi, and J. M. Elmirghani, "25 Gbps mobile visible light communication system employing fast adaptation techniques," in *18th International Conference on Transparent Optical Networks (ICTON)*. IEEE, 2016, pp. 1–7.

[19] E. Leitgeb, M. Loschnigg, U. Birnbacher, G. Schwarz, and A. Merdonig, "High reliable optical wireless links for the last mile access," in *10th Anniversary International Conference on Transparent Optical Networks, ICTON*, vol. 4. IEEE, 2008, pp. 178–183.

[20] E. Leitgeb, J. Bregenzer, P. Fasser, and M. Gebhart, "Free space optics-extension to fiber-networks for the "last mile"," in *15th Annual Meeting on Lasers and Electro-Optics Society, LEOS.*, vol. 2. IEEE, 2002, pp. 459–460.

[21] N. Guo, R. C. Qiu, S. S. Mo, and K. Takahashi, "60-GHz millimeter-wave radio: Principle, technology, and new results," *EURASIP journal on Wireless Communications and Networking*, no. 1, pp. 48–48, 2007.

[22] A. Kamboj, R. K. Mallik, M. Agrawal, and R. Schober, "Diversity combining in FSO systems in presence of non-gaussian noise," in *International Conference on Signal Processing and Communications (SPCOM)*. IEEE, 2012, pp. 1–5.

[23] B. He and R. Schober, "Bit-interleaved coded modulation for hybrid RF/FSO systems," *Transactions on Communications*, vol. 57, no. 12, 2009.

[24] F. Gebali, *Analysis of computer networks*. Springer, 2015.

[25] M. Haugh, "Generating random variables and stochastic processes," *Monte Carlo Simulation: IEOR EA703*, 2004.